TERRESTRIAL LIDAR IMAGING AND FRACTURE ANALYSIS OF THE WOODFORD SHALE; WESTERN ARKOMA BASIN, OKLAHOMA

by

ROBERT WILLIAM WENCEL

IBRAHIM ÇEMEN, COMMITTEE CHAIR
MARCELLO MINZONI
BO ZHANG
JAMES PUCKETTE

A THESIS

Submitted in partial fulfillment of the requirements
For the degree of Master of Science
in the Department of Geological Sciences
in the Graduate School of
The University of Alabama

TUSCALOOSA, ALABAMA

2021

ABSTRACT

Since the late 1990s horizontal drilling and hydraulic fracturing of Devonian shales in the mid-continent region, such as the Woodford Shale, has revolutionized gas exploration in the United States. These two methods are reliant on robust predictive reservoir models, particularly addressing the geometry, spacing, and density of complex natural fracture networks within the otherwise tight shale. However, the natural fractures within the Woodford Shale have not been rigorously studied despite their importance to fluid flow and ultimately recovery of hydrocarbons. Most of the subsurface fracture mapping of the Woodford has been done using 3D seismic data and seismic attribute analysis. This study applies terrestrial Light Detection and Ranging (LiDAR) to study natural fracture patterns of two Woodford outcrops located in the Arkoma Basin, southeastern Oklahoma. One outcrop is located south of the town Wapanucka, and the other outcrop is east of the town Atoka.

The high-resolution images obtained from terrestrial LiDAR reveal fracture spacing and fracture density allowing the quantitative assessment of how these fractures vary in different sections of the Woodford Shale where bedding thickness, mineralogy, and degree of deformation (folding) differ significantly. In this study we evaluate whether a statistical relationship exists between bedding thickness and the mineralogy (i.e., silica content vs organic content), fracture spacing, and fracture density of shale beds. Preliminary results suggest that thicker beds contain larger fracture spacing and smaller fracture density. The results of this study will help us to 1) better understand geometry, origin, and distribution of natural fractures in the Devonian

Woodford shale in the Mid-Continent region of the United States and in other parts of the world; and 2) develop more realistic reservoir models for improved hydraulic fracturing methods.

ACKNOWLEDGEMENTS

I would like to thank my advisor Dr. Ibrahim Çemen for giving me the opportunity to pursue my master's degree at the University of Alabama. Without all the help and guidance that he provided me I would not have been able to complete this project. I would also like to thank my advisory committee; Dr. Marcello Minzoni, Dr. Bo Zhang, and Dr. James Puckette for all the help and edits that they provided me along the way. I would also like to thank Dr. Matt Wielicki and my fellow students Sam Walker and Ryan Culp for their help preparing my samples for the XRF data. This addition to the project was of great use and would not have been possible without their help. Finally, I would like to thank Brian Cardott of the Oklahoma Geological Survey for his help in locating the outcrops for this study and providing me with necessary information to begin this project. I would also like to thank the Department of Geological Sciences, the University of Alabama graduate school, and the Geological Sciences Advisory Board (GSAB) for providing the funding for this project. Without the help of these scholarships, I would never have been able to collect all my data.

CONTENTS

LIST OF FIGURES

CHAPTER I

INTRODUCTION

INTRODUCTION

The Arkoma Basin is one of several Carboniferous foreland basins in the southern midcontinent extending from west-central Arkansas to southeastern Oklahoma (Fig. 1). It is one of the most prolific petroleum producing basins in North America (Suneson, 2012), and in recent decades has been targeted for horizontal drilling in the Woodford Shale which is the most prominent source rock and unconventional reservoir within the basin (Cardott, 2012). Outcrops of Woodford Shale in southeastern Oklahoma contain complex natural fracture networks which can be used for subsurface analogues in order to facilitate oil and gas production. This study applies terrestrial Light Detection and Ranging (LiDAR) (Fig. 2) to create 3D models and precise, high resolution, images of outcrop scale natural fracture patterns in order to quantitatively analyze information about bedding thickness and its relationship between fracture spacing and fracture density. Two outcrops in the southwestern Arkoma Basin were imaged with the use of terrestrial LiDAR and analyzed for these relationships.

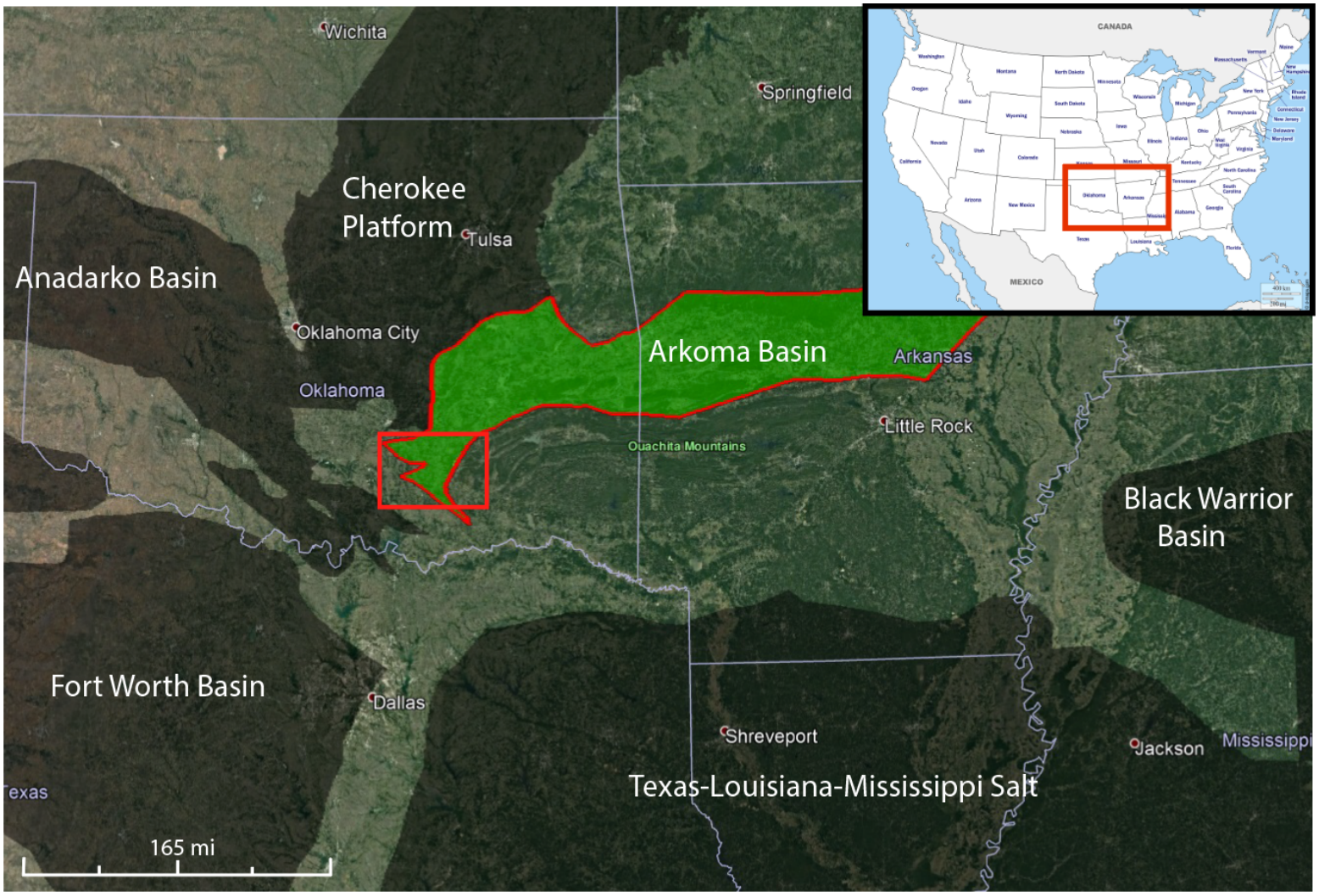

Figure 1- Sedimentary Basins within the midcontinent region including the Arkoma Basin. The study area for this project is marked with a red square in the southwestern portion of the Arkoma Basin in southeastern Oklahoma.

STATEMENT OF PURPOSE

Since the late 1990s horizontal drilling of fractured Devonian Shales such as the Woodford Shale has revolutionized gas exploration in the mid-continent region of the United States. Horizontal drilling methods are reliant on the complex natural fracture networks within the otherwise tight shale unit. However, the fractures are also artificially induced through hydraulic fracturing. The natural fractures within the Woodford Shale have not been rigorously studied despite their importance to fluid flow and ultimate recovery of hydrocarbons (Ghosh,

2017). This study is aimed to provide a better understanding of the natural fracture spacings and densities within the Woodford Shale at the outcrop scale and their relationship to varying bedding thicknesses, silica content, and degree of deformation. This relationship is quantitively evaluated with the use of terrestrial LiDAR, which decreases uncertainties introduced by measurement errors in the Woodford's complex fracture network (Fig. 2).

Figure 2- Terrestrial LiDAR setup in front of the Woodford Shale at the Wapanucka outcrop located ~2 miles south of Wapanucka, Oklahoma.

RESEARCH QUESTIONS

This study has been conducted to seek insights to the following research questions:

(1) Is there a relationship between natural fracture density/spacing and the thickness of the beds in each outcrop? This relationship has been tested in the past but has yet to be studied in depth with the use of LiDAR images in the two selected outcrops of the Woodford Shale

(2) Does the mineralogy and organic content vary vertically in the outcrops and between the outcrops, and if so, do these factors influence the formation and distribution of natural fractures?

(3) What effect, if any, does the localized folding superimposed on the vertical limb of the fold in the Atoka outcrop (Fig. 3) affect the natural fracture networks?

Additionally, this study aims at a better understanding of how the fracture networks in the two outcrops studied in this project relate to other Woodford outcrop studies in different areas of southern Oklahoma as well as contribute to the understanding of the application of terrestrial LiDAR to outcrop evaluations of natural fracture spacing and density.

STUDY AREA

The Arkoma Basin extends from the Gulf coastal plain of Arkansas westward roughly 400 km to the Arbuckle Mountains in south-central Oklahoma (Sutherland, 1988) (Fig. 1) and runs parallel and adjacent to the Ouachita fold and thrust belt. The two outcrops in the study are located in the southwest portion of the Arkoma Basin in southeastern Oklahoma in Atoka and Wapanucka counties (Figs. 1 and 3) and will be referred to as the Atoka and Wapanucka outcrops. Although several outcrops of the Woodford have been analyzed for their natural fracture patterns in southeastern Oklahoma by previous studies (Ataman, 2008; Hanzel, 2012), these two remained unstudied in terms of their natural fracture patterns.

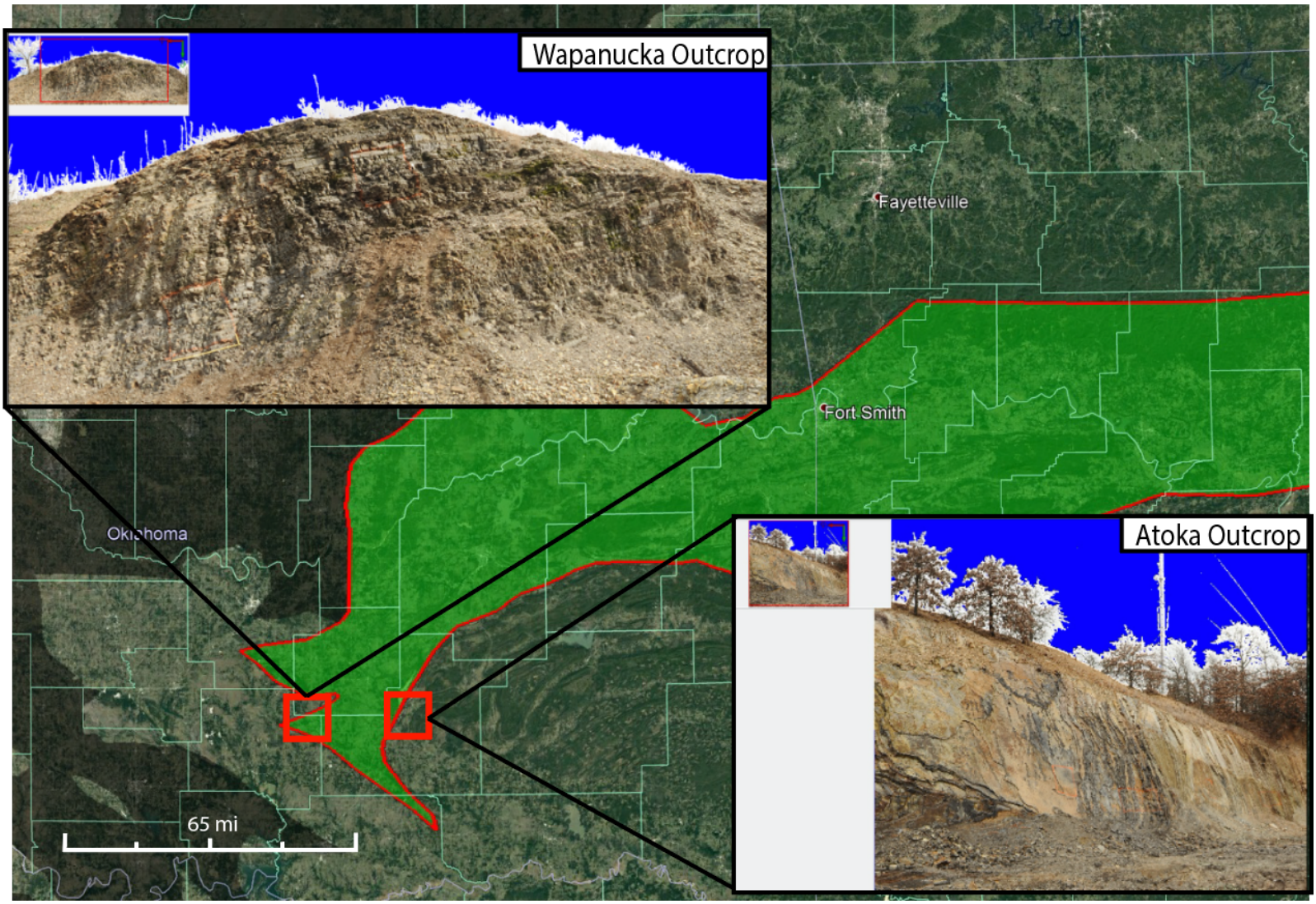

Figure 3- Study area for this project including locations and LiDAR images of Wapanucka and Atoka outcrops. The Wapanucka is located ~2.5 miles southwest of the town Wapanucka, OK and consists of gently dipping Woodford Shale. The Atoka outcrop is located ~2 miles southeast of the town Atoka OK, and consists of heavily deformed Arkansas Novaculite.

The Atoka outcrop is located near scratch hill roughly 2 miles southeast of the town of Atoka at 34 22'31.63" N and 96 06'35.77" W location, in the frontal fold belt of the western Ouachita Mountains area. The outcrop is steeply dipping and heavily deformed with superimposed folding and is unique in that it consists of the Arkansas Novaculite (Fig. 13), a silica rich time-stratigraphic equivalent of the Woodford Shale located in the Ouachita Mountains (Cardott and Lambert, 1985). The Wapanucka outcrop is located about 2.5 miles

southwest of the town of Wapanucka at 34°20'47.07"N 96°26'4.47"W location. The Wapanucka outcrop consists of gently dipping, uniform beds of Woodford Shale and is only slightly deformed compared to the heavily deformed Atoka outcrop (Fig. 3). Both outcrops contained pyrite and phosphate nodules which only occur in the upper portion of the Woodford (Cardott, 2007; Slatt et al., 2011; Milad and Slatt, 2017; Hanzel, 2012; Mnich, 2009; Cardott, 2012; Portas and Slatt, 2010; Portas, 2009). This indicates that the outcrops are stratigraphically part of the silica rich upper Woodford member (Fig. 14).

IMPORTANCE NATURAL FRACTURE STUDIES

Natural fracture studies are important for unconventional gas reservoirs by providing insight into fracture orientations and connectivity which play a crucial role in determining primary migration paths for hydrocarbon accumulations. The analysis of fracture relationships is useful for creating fluid flow models as well as improving drilling targets in unconventional reservoirs. Terrestrial LiDAR imaging of outcrops for their natural fracture patterns has been increasingly popular in the petroleum industry due to LiDAR's high precision and high-resolution images that provide meaningful clues to fracture characteristics in the subsurface (Bellian, 2002; McCaffery et al., 2005; Adams et al., 2009; Zahm et al., 2010; Hanzel, 2012; Clark and Cemen, 2015). It is important to study natural fracture characteristics in the Woodford specifically as it is recognized as one of the most important unconventional gas reservoirs in the mid-continent region. With natural fractures directly controlling permeability, a good understanding of their geometries is crucial to increasing gas production (e.g., Ataman; 2008. Hodgetts, 2012; Clark and Cemen, 2015).

METHODS

a. Terrestrial LiDAR

The outcrops in the study area (Fig. 2) were analyzed for their natural fracture patterns with the use of terrestrial Light Detection and Ranging (LiDAR). The availability of ground-based laser scanner systems over the last decade has opened up new possibilities for the determination of fracture surface orientation in rock outcrops and has become a popular tool for modeling petroleum reservoir analogues in their natural outcrops (Hodgetts, 2012; Olariu et al., 2008). LiDAR creates 3D models of objects by emitting lasers to illuminate a target and analyzing the response times of reflected pulses (Fig. 4). Surface geometry of the outcrop is remotely captured in the form of dense 3D point clouds. Point cloud data or "clouds" are enormous volumes of point data created by the laser scanner systems (Olariu et al., 2008).

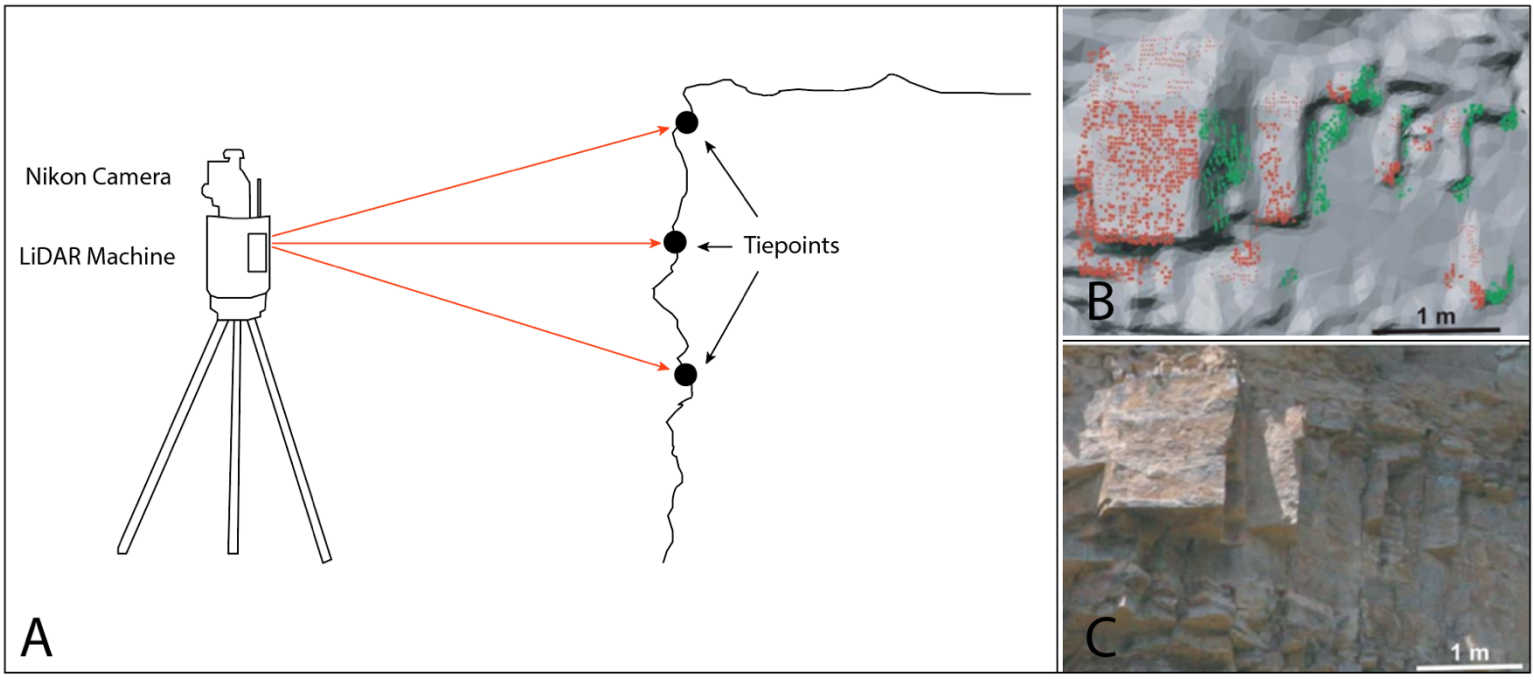

Figure 4- (A) Rough sketch of terrestrial LiDAR setup and imaging process in relation to outcrop. (B) First 360-degree image acquisition scan completed by LiDAR that produces rough scan of everything in the machines surrounding area. (C) Second color acquisition scan done with the mounted Nikon camera in order to add color and detail to first panorama scan done with the terrestrial LiDAR machine.

Ground based laser scanners have proven very useful for acquisition of high-quality, high resolution, three-dimensional terrain data from outcrops (Xu et al., 2000; Bellian et al., 2002; McCaffery et al., 2005; Clark and Cemen, 2015). There are many models of terrestrial LiDAR, but the model used in this study is the RIEGL VZ-400. RIEGL Laser Measurement systems is an Austria based company that is an industry leader in 3D laser scanners. They manufacture a variety of LiDAR scanners including terrestrial, airborne, and unmanned scanners. The VZ-400i terrestrial model was used here as it is designed for high accuracy at extra high speed, measuring up to 122,000 data points per second at an accuracy of 5mm and can image objects from as far as 550m and as close as 1.5m. The scans conducted during this study were obtained at about 10m distance from the outcrop. The resolution of the 3D spatial relationships is derived from the user controlled horizonal and vertical step widths as the laser steps across the surface, maxing out at .0024 for the VZ-400 (Clark, 2015).

There are multiple pieces needed in order to run terrestrial LiDAR machines in the field (Fig. 5). To capture imagery data from the outcrops a tripod is used to mount the LiDAR machine. The LiDAR is then mounted with a Nikon camera that is used for the color acquisition scan. A car battery is needed to power the machine and is connected by cables that resemble jumper cables for a car with one end connecting directly into the LiDAR. Finally, a field laptop is needed to run RiSCAN Pro, which is the program used to control the machine in the field as well as observe and analyze the high-resolution images for their natural fracture network measurements in the laboratory.

The process of obtaining 3D models and high-resolution images from terrestrial LiDAR is a multistep process. An initial 360-degree panorama scan is needed to obtain a 3D model of everything in the machine's surroundings (Fig. 4-B). To do this, the machine conducts an initial scan where it emits lasers to illuminate a target. The lasers are then reflected and analyzed for their response time to produce a 3D model of everything in the surrounding area. The LiDAR will then conduct a color acquisition scan using the mounted Nikon camera in order to add color to the model (Fig. 4-C). Once the panorama 3D model is obtained, specific areas can be targeted to image at even higher resolutions. Imaging specific areas in the outcrop follows the same process as the initial 3D LiDAR scan; first scanning the designated area by emitting lasers and analyzing the response time, followed by a color acquisition scan.

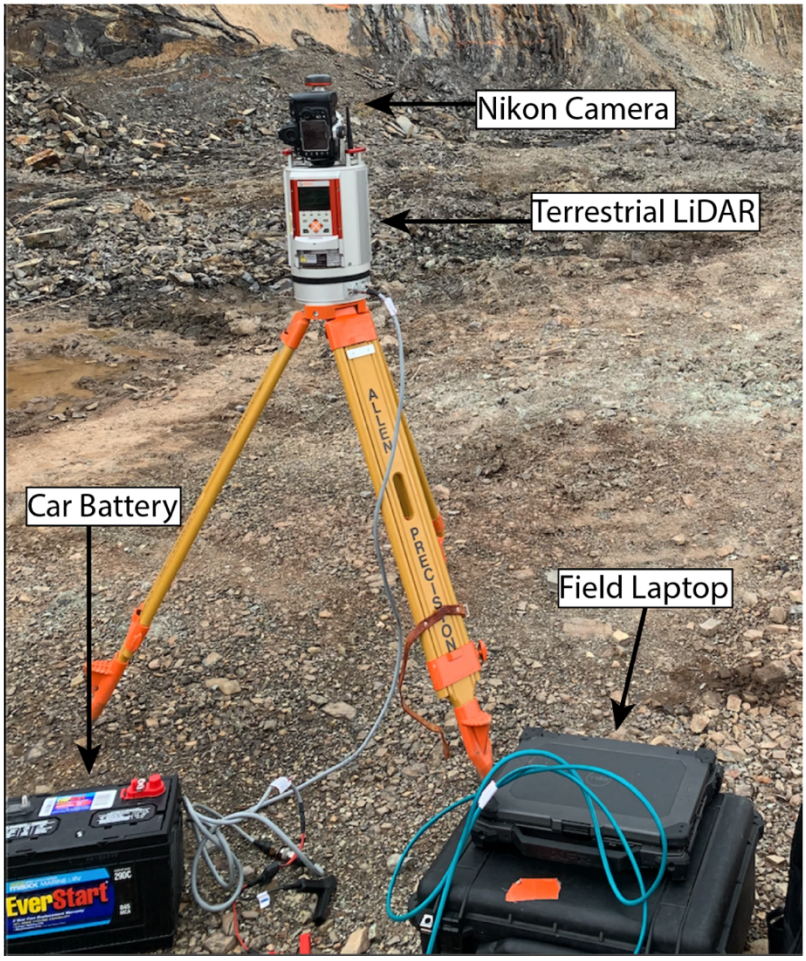

Figure 5- Field setup for terrestrial LiDAR. LiDAR machine is mounted on a tripod and a Nikon camera is attached to the top of the LiDAR. A car battery is used to power the machine and a laptop is connected to the LiDAR in order to control the machine with the use of RiSCAN Pro.

In order to get the highest resolution images possible, it is necessary to push the machine close to its limits without overloading it (Fig. 6). Because the initial panorama 3D models require

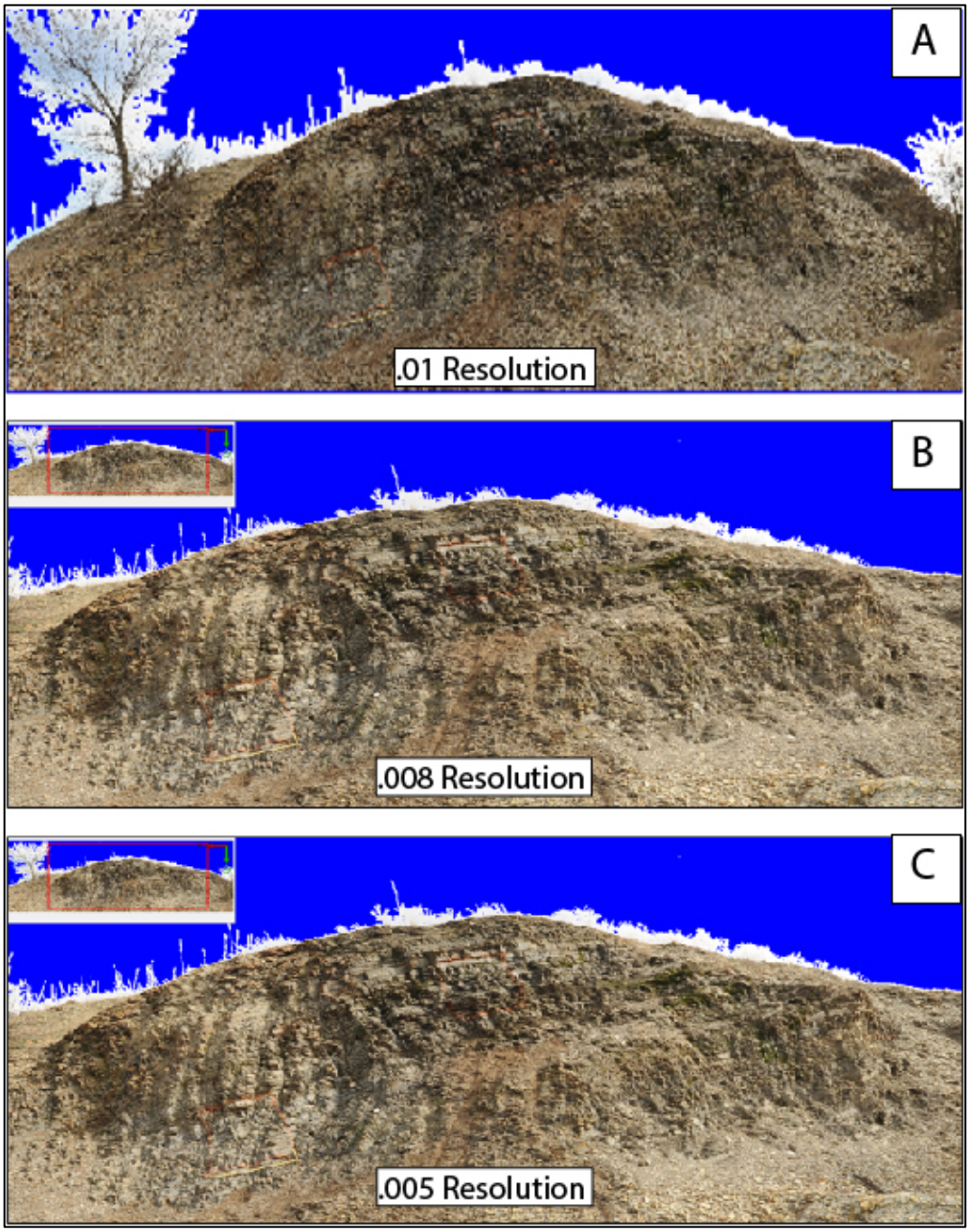

Figure 6- Outcrop scale LiDAR scans of the Wapanucka outcrop done at resolutions of .01 degrees (A) .008 degrees (B) and .005 degrees (C). This illustrates the importance of scanning outcrops and inventory squares at the highest resolution possible without overloading the LiDAR machine in order to obtain the best images for fracture analysis.

a great amount of data, they are created at the defaulted horizontal and vertical resolution of .08 degrees in order to preserve memory in the machine. Once the 3D models were obtained the outcrops were highlighted for a secondary scan in order to obtain high resolution images of the entire outcrop. Because the outcrop scan was targeting a specific area within the 3D model, the resolution was increased to .005 degrees which allowed the highest resolution image possible at that data size (Fig. 6). Once the outcrop images were obtained, the marked 1m inventory squares were scanned individually at the highest resolution of .002 degrees. The higher the resolution the more uncertainties are

reduced (Adams et al., 2009; Ahmadzamri et al., 2014; Minisini et al., 2014). A .002-degree scan provided the highest resolution possible without crashing the machine allowing the best possible image to quantitatively analyze natural fracture patterns.

b. Fracture Analysis

Fractures and other mechanical discontinuities act as preferable fluid pathways in the subsurface, therefore strongly controlling fluid flow in hydrocarbon reservoirs (Zeeb et al., 2013). An essential step for reservoir characterization is the acquisition of fracture network data and the subsequent upscaling of their statical properties (Long et al., 1982; Jackson et al., 2000; Blum et al., 2009). A common method to evaluate the degree of fracturing in the subsurface is the characterization of fracture networks from outcropping subsurface analogues, well cores, or image logs (Dershowitz and Einstein, 1988; Priest, 1993; Mauldon et al., 2001; Bour et al., 2002; Laubach, 2003, Blum et al., 2007; Guerriero et al., 2011). This process includes the acquisition of geometric data from fractures and its subsequent analysis to find statistical distributions and relationships between parameters (Priest, 1993; Blum et al., 2005, Toth, 2010). Developing accurate geologic models of fracture relationships can help predict zones for successful stimulation or "sweet spots" within unconventional reservoirs by improving predictions in well placements.

Several studies have applied terrestrial laser scanning and modelling techniques to characterize fractures (Olariu et al., 2008; Zahm et al., 2010; Wilson et al., 2011; Pearce et al., 2011; Hanzel, 2012; Clark, 2015; Ginter, in prep). These studies provide insight into the usefulness of terrestrial LiDAR toward fracture studies and models. Zeeb et al (2013) outlines three methods that can be used at the outcrop scale to measure fracture network characteristics. These methods include scanline sampling, window sampling, and circular scanline sampling.

Each method varies in its application and the parameters they provide meaning that each has its advantages and disadvantages.

During this study, the window sampling method was applied because common applications of this method are a) the analysis of outcropping rocks for their subsurface analogues (Belayneh et al., 2009) and b) characterization of fracture networks using remote sensing data (Zeeb et al., 2013). The window sampling method works by estimating the statistical properties of fracture networks by measuring parameters from all fractures present within the selected sampling area. There are generally three types of sampling biases that affect the window sampling method: (1) orientation (2) truncation, and (3) censoring biases. To apply this method, the outcrops were

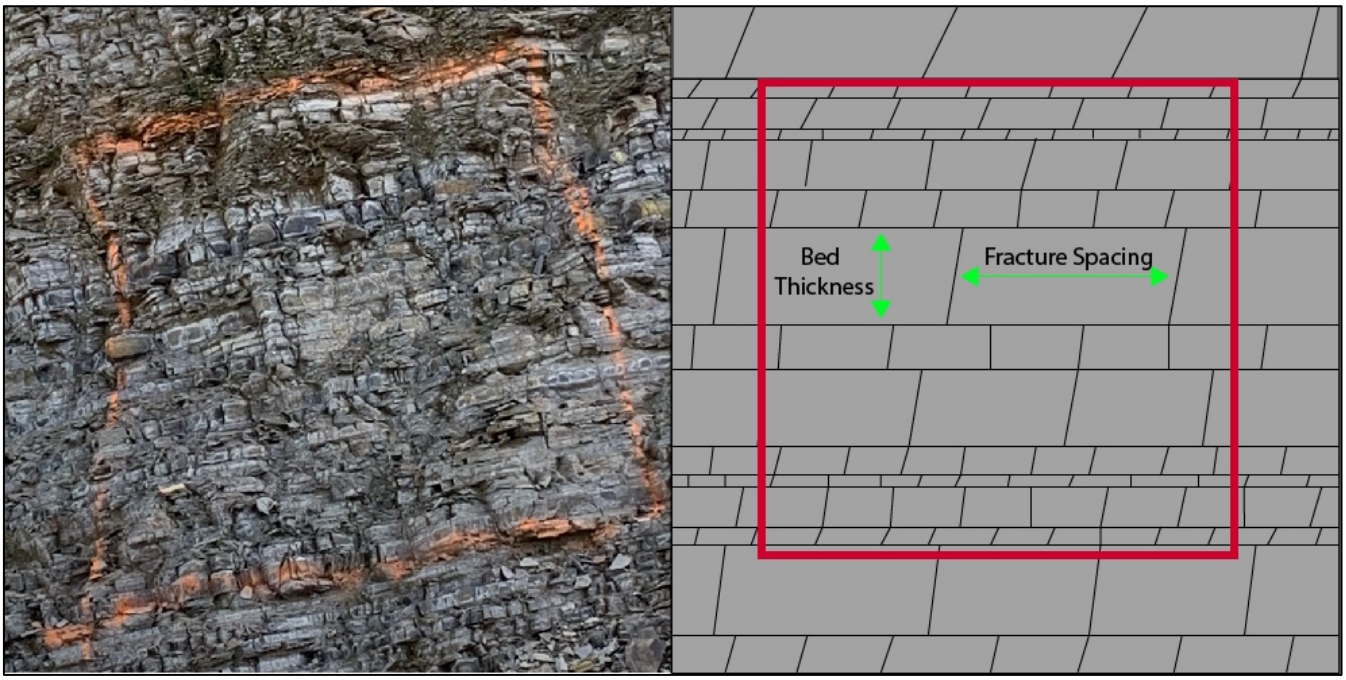

Figure 7- 1m inventory square of Woodford Shale marked in order to locate specific sections of Woodford where bedding thickness and fracture spacings varied significantly (Left). Cartoon showing the measurements taken for bed thickness and fracture spacings in order to assess if there is a relationship between the two parameters (Right).

marked with 1m inventory squares targeting areas where bedding thicknesses varied in order to analyze fracture spacings and densities in different bed thicknesses (Fig. 7).

The window sampling method was applied with the use of the RiScan Pro computer program using the high-resolution LiDAR images. The program was used to precisely measure the thickness of every bed within the inventory square as well as analyze fracture spacing and fracture density in each bed, allowing a relationship to be established between fracture spacing and bedding thickness as well as fracture density and bedding thickness. Fracture spacing and fracture density often correlate with bed thickness (Laderia and Price, 1981; Wu and Pollard, 1995; Ji and Saruwatari, 1998; Schiopfer et al., 2011; Clark, 2015) with fracture spacing increasing as bedding thickness increases and fracture density decreasing as bedding thickness

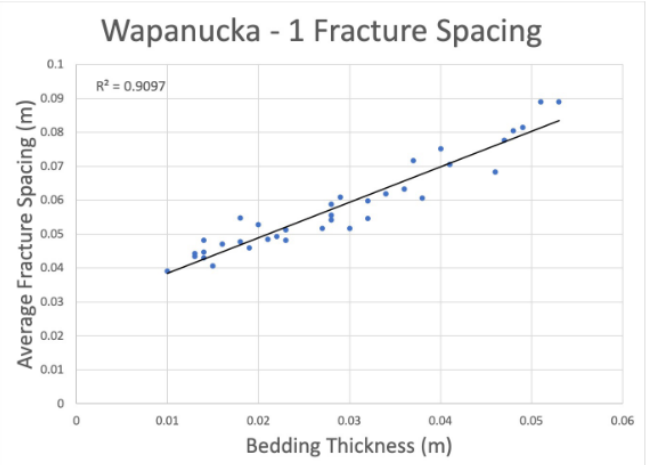

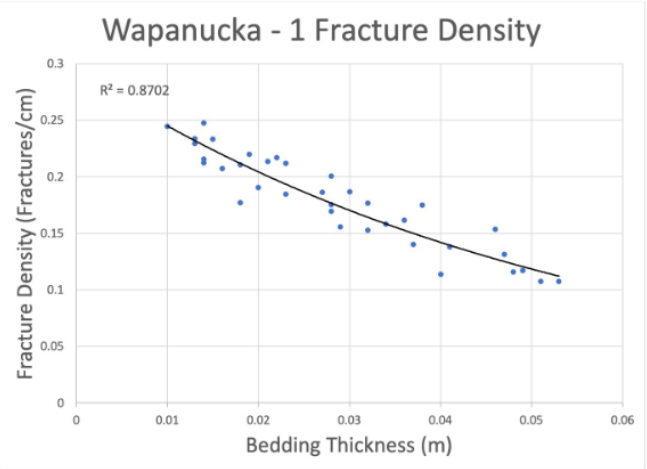

Figure 8- Fracture spacing and fracture density graphs in relation to bedding thickness at the Wapanucka outcrop. Fracture spacings are represented as an average of all fracture spacings in the bed and is measured in meters. Fracture density is a measurement of the number of fractures present in each bed within the inventory square and is represented as # of fractures per cm.

increases. This linear relationship ideally holds true within a homogenous bed free from defects or flaws including cracks, fractures, impurities, or fossils (Clark, 2015). However, some studies

propose a linear relationship is too generic in principle (Narr and Lerche, 1984; Dershowitz and Herda, 1992; Narr, 1996) due to impurities within the rock unit creating variances in the relationship.

c. Geochemical Analysis

During this study, a Geochemical analysis was conducted using samples of Woodford Shale and its stratigraphic equivalent; Arkansas Novaculite. These samples were collected at varying stratigraphic levels at each outcrop where bedding thicknesses varied (Fig. 9). These samples were then used for a petrographic analysis using thin sections as well as whole rock analysis using X-Ray Fluorescence (XRF). This was done so in order to assess the amount of silica in varying sections of each outcrop to determine if there was a relationship between bedding thickness and silica content, and ultimately silica content and fracture spacing and density. Five different samples were collected from the Wapanucka outcrop and six were collected from the

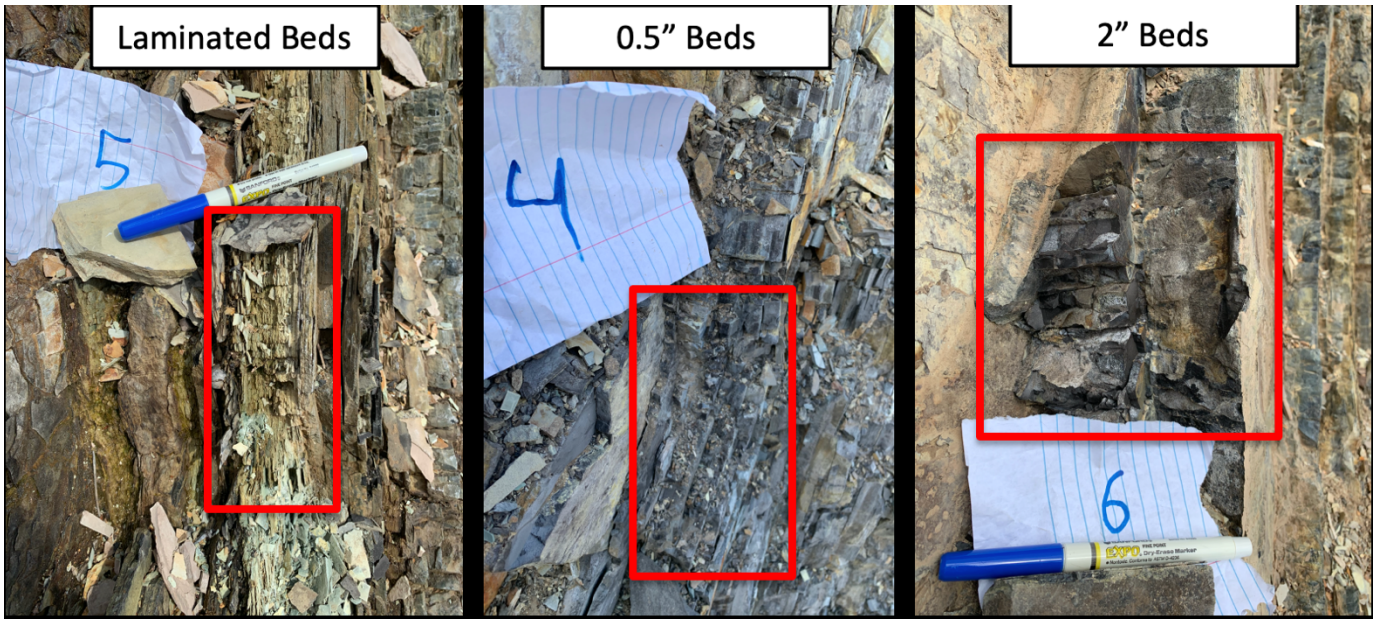

Figure 9- Different bedding thicknesses that were sampled in order to prepare thin sections for a petrographic analysis and glass beads for XRF data. Bedding thicknesses range from thinly laminated (Left), upwards of 2" thick (Right).

Atoka outcrop with bedding thicknesses of these samples ranging from thinly laminated to 2" thick.

a. Petrographic Analysis

Petrography of organic shales via incident light microscopy is defined as the study of solid matter in sedimentary rocks (Suarez-Ruiz et al., 2012) and has a broad application to shale petroleum systems such as the ability to identify various types of solid and organic components in shale plays (Hackley and Cardott, 2016). The origin and form of quartz has significant implications for interpretations of depositional environments, diagenetic pathways, mechanisms of porosity reduction, and rheological mechanical-property evolution of rock samples (Peng et al., 2020).

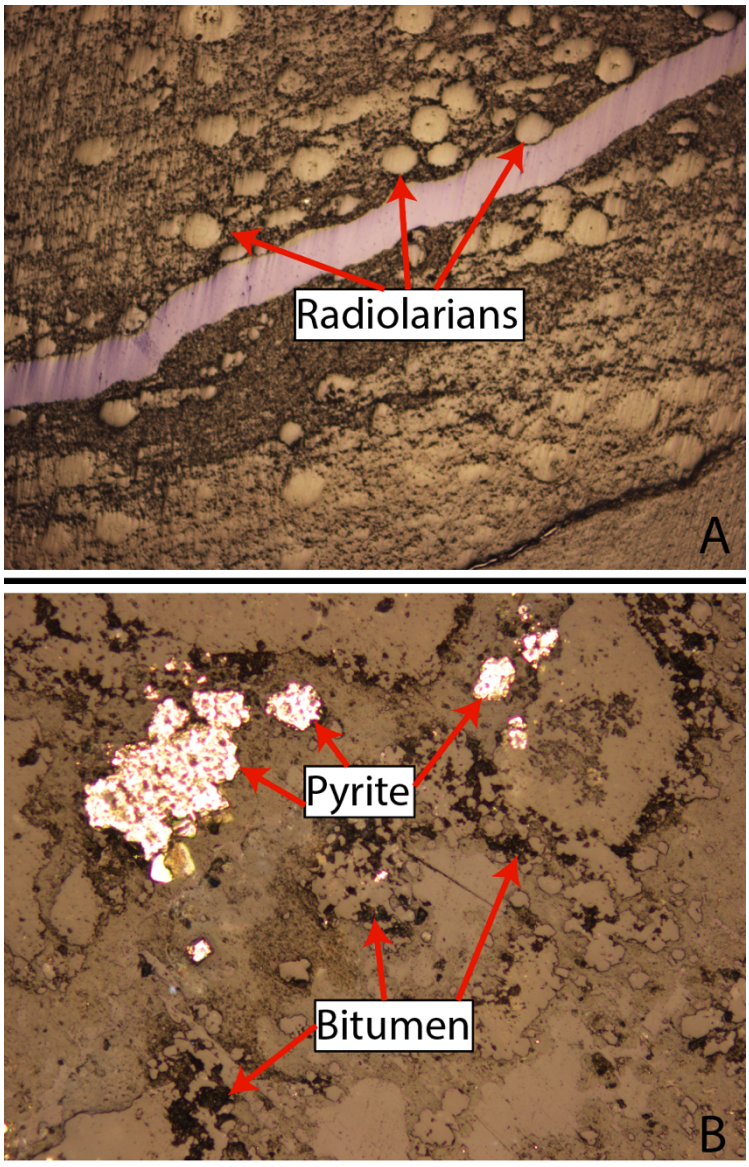

Figure 10- Thin section images taken from Woodford Shale samples showing biogenic silica within the Woodford being sourced from radiolarians as well as pyrite and solid bitumen.

Samples were collected from both outcrops at different stratigraphic levels where bedding thickness varied. Thin sections were made from selected samples to analyze the silica content at varying stratigraphic levels and bedding thicknesses (Fig. 10). Eight samples were sent off for thin section

preparation, five from the Atoka outcrop and three from the Wapanucka outcrop. Samples were sent to TPS Enterprises LLC in Bellaire, Texas for polished thin section preparation. Polished thin sections could only be prepared from samples that had bedding thicknesses of ~1" to ~3". Therefore, thinly laminated samples were not observed in thin section.

b. Whole Rock analysis

Chemical compositions and the mineral modal compositions have been a principal information for geochemical studies (Kon et al., 2011). For the analysis of chemical composition of rock samples, X-ray fluorescence (XRF) spectroscopy on glass beds created from rock samples has been widely used because of both the high reliability in the resulting data (Norrish and Hutton, 1969). There are many advantages to using XRF to analyze rocks and minerals including the versatility of the instrumentation and methods that can be developed to satisfy a wide variety of needs (Johnson et al., 1999). Nine samples were prepared for XRF analysis, five from the Atoka outcrop and four from the Wapanucka outcrop, in order to observe the silica content in different sections of the outcrops where bed thicknesses varied. Bed thicknesses that were analyzed range from thinly laminated to ~2" thick.

To prepare samples for XRF analysis glass beads were created from all nine rock samples (Fig. 11). To do this, rock samples were powdered with the use of a puck and mill in a shatter box. 3.5g of the rock powder was vigorously mixed together with 7.0g of dilithium tetraborate (at a ratio of 1:2) and emptied into a graphite crucible. Once all crucibles were filled, they were placed in a preheated oven at 1000 C for 10 minutes allowing fusion to occur, and then removed to cool. Once fully cooled the beads were taken out of the crucible and powdered once again using the puck and mill in a shatter box. The resulting glass bead powder was then placed in a crucible, this time without any dilithium tetraborate, and fused at 1000 C for another 10 minutes in a preheated oven.

Figure 11- Glass beads prepared from samples in order to obtain XRF data.

Following the second fusion the tops of the cooled beads were labeled with an engraver with their respective sample ID. The bottom portion of the beads were polished on a grinding wheel and then ground on silicon grit paper with alcohol to remove any metal from the grinding wheel. Next, the polished beads were washed in an ultrasonic cleaner, first with water and then with alcohol. Finally, the beads were wiped dry and stored in sample bags to be shipped off for analyzation in an XRF spectrometer at Pomona College in Claremont, California.

CHAPTER II

GEOLOGIC OVERVIEW

ARKOMA BASIN

The Arkoma basin is a peripheral foreland basin (Allen et al., 1985; Miall, 1995; DeCelles and Giles, 1996) that presently extends from the Gulf Coastal plain in Arkansas roughly 400 kilometers westward to the Arbuckle Mountains in south-central Oklahoma (Sutherland, 1988). It formed due to the collision of the North American and Gondwanan plates starting in the Early Mississippian and ending in the Middle Pennsylvanian with much of its sedimentary and structural history being closely related to the Ouachita fold-and-thrust belt (Suneson, 2012). The foreland region along the entire length of the Ouachita orogenic belt generally shared a common history of rifted margin sedimentation during the early to middle Paleozoic followed by foreland basin development induced by convergent tectonism during the late Paleozoic (Flawn et al., 1961; Graham et al., 1975; Thomas, 1985; Houseknecht, 1984).

a. Tectonics of the Arkoma Basin

There are many studies that focus on the tectonic evolution of the Arkoma Basin and the Ouachita Mountains (Walper, 1977; Cox, 1988; Haley and Stone, 1995; McBee, 1995; Brown; 1995; Suneson, 2012). The development of the basin can be subdivided into three stages (Fig. 12): (1) rift and drift stage (2) a collision stage, and (3) uplift and erosion stage (Xu et al., 2009).

From the Cambrian to Devonian the area was a long-lived shelf (north), slope, and basin (south). Subsidence of the foreland basin began in the Mississippian as response to thrusting and tectonic loading and continued through the Pennsylvanian due to continued thrusting and tectonic loading until the late Atokan to early Desmoinesian when the Ouachita tectonic belt was uplifted above sea level (Suneson, 2012).

A peripheral foreland basin (PFB forms adjacent and parallel to a collisional mountain belt on the subducting plate during continent-continent collision. In the case of the Arkoma Basin this is the Ouachita fold-and-thrust belt. Combining tectonic models of Wickham et al. (1976);

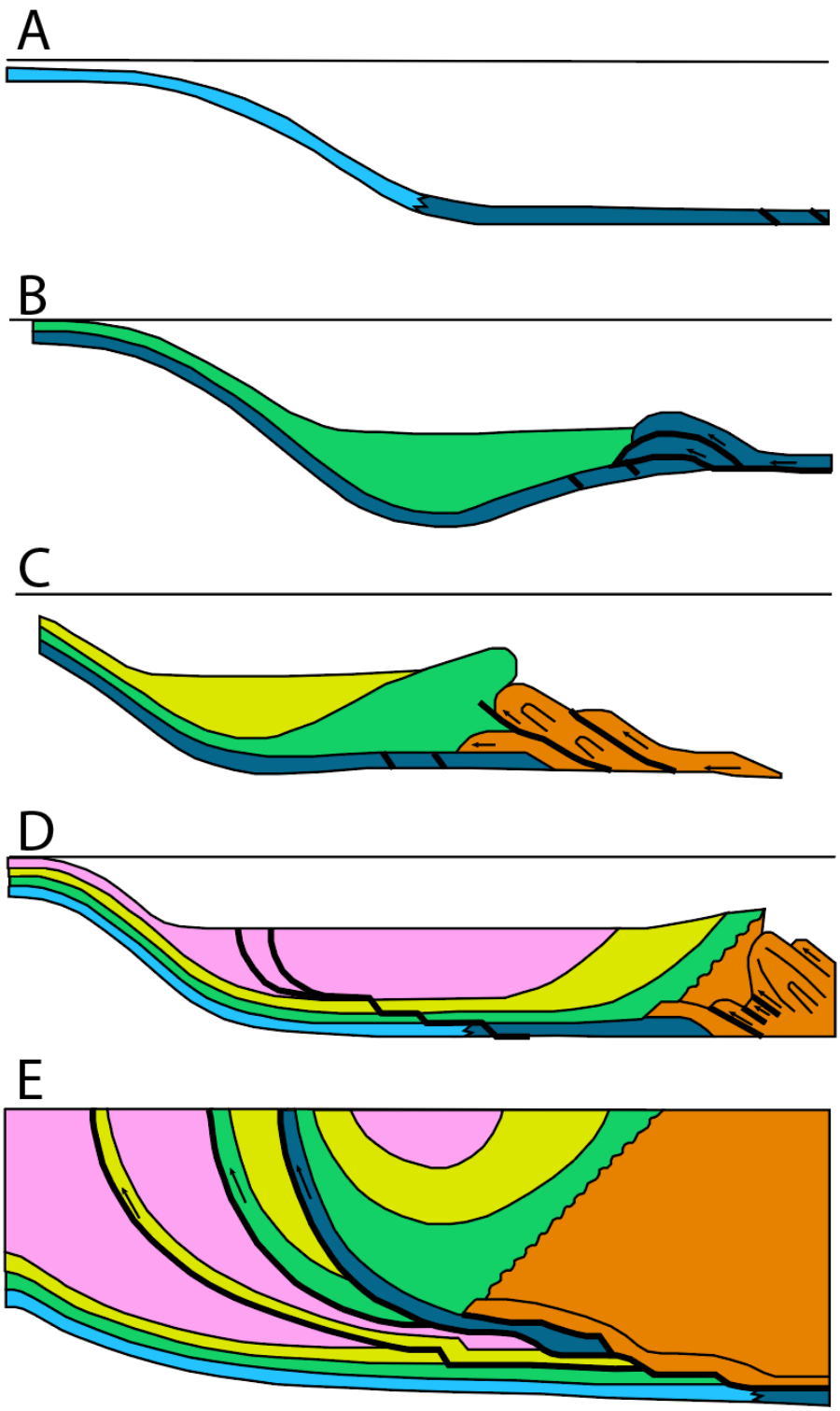

Figure 12- Tectonic evolution of the Arkoma Basin. (A) Stable shelf from Cambrian to Devonian. (B) Subsidence begins in early Mississippian in response to thrusting and tectonic loading. (C) Subsidence continues through Pennsylvanian as thrusting and tectonic loading progresses. (D) Continued thrusting into middle Pennsylvanian shifts axis of deposition north. (E) Middle Pennsylvanian, Ouachita tectonic belt is uplifted ending basin formation. (modified from Suneson, 2012).

Houseknecht et al., (1986); Allen et al. (1986) and Suneson, (2012), much of the geology of the Arkoma basin can be explained (Fig. 12). For example, a PFB stratigraphic sequence typically reflects the filling of the basin and the progression from deep to shallow water deposits. This is exhibited in the Arkoma basin by the transition from middle Atokan turbidite to deep marine basinal deposits to late Atokan shallow marine fluvial deltaic deposits. Sedimentation along the axis of the basin is common in PFBs. Most of the turbidites in the Ouachita belt trend east to west which is parallel to the axis of the Arkoma Basin. There are so many characteristics of PFBs observed in the Arkoma Basin geology that characteristics that have not been positively identified in the past are currently being investigated. These features are foreland bulge, reactivated normal and thrust faults (Suneson, 2012), although Mazzulo et al (2011) has proposed that features within Mississippian strata in northern Oklahoma and adjacent states indicates the presence of a forebulge resulting from the Ouachita orogeny.

Structurally, the Arkoma Basin can be subdivided into two regions. The southern region is dominated by compressional features such as thrust core anticlines which act as traps for major gas fields in the basin. The northern region consists of “drape” anticlines over middle Atokan normal faults (Suneson, 2012). The boundaries of the basin are well defined by other major structures. The southern basin margin is defined by Ouachita frontal thrust faults, specifically the Choctaw fault in Oklahoma and the Ross Creek fault in Arkansas. These two faults are defined as leading-edge thrusts of the Ouachita fold-thrust belt. The eastern and southwestern ends of the basin are defined by Cambrian or older grabens that were subsequently inverted (Houseknecht et al., 2014). The eastern graben is the Mississippi Valley graben, also referred to as the Reelfoot rift, and the southwestern graben is the southern Oklahoma aulacogen. Both of which formed as failed-rift arms along the southern margin of Laurentia (Viele and Thomas, 1989; Thomas, 2004)

during the fragmentation of the supercontinents Rodinia. Finally, the northern boundary is well defined by the Ozark Uplift and the northeast Oklahoma platform (Houseknecht et al., 2014).

b. Sedimentation

The Arkoma Basin contains a great thickness of sedimentary rocks whose ages range from upper Cambrian to upper lower Pennsylvanian (Kont, 1991) (Fig. 13). Much of these deposits consist of pre-Mississippian carbonate shelf deposits and organic-rich marine shales as well as early Pennsylvanian fluvial deposits (Perry, 1995). For much of its history (Cambrian to Early Mississippian), the Arkoma Basin was depositionally part of a broad stable shelf along a North American passive margin (Fig. 12a). However, during the Mississippian and Pennsylvanian (Fig, 12b, c, d, and e), depositional patterns varied greatly depending on the tectonics influence on carbonate environments and intermittent introduction of terrigenous clastics (Sutherland, 1988).

From the Cambrian to early Mississippian the Arkoma Basin was part of a stable shelf along a passive continental margin (Fig 12a). During this period a thick sequence of mostly shallow water carbonates was deposited on the shelf and thinner deep-water black shales and cherts accumulated in the basin. Beginning in the middle Atokan flexural down warping of the south margin shelf resulted in the collapse of the Ouachita trough and lithic arenites were introduced into the developing trough from the east. Further compression of the Ouachita orogeny shifted the axis of deposition northward in the Desmoinesian. Continued subsidence of the basin

throughout the Desmoinesian introduced extensive deltaic deposits from the north and northeast where the Appalachian fold-thrust belt was developing (Sutherland, 1988).

Progressive down warping of the basin ended with renewed uplift and folding of the Ouachita fold-thrust belt resulting in the depocenter being shifted even farther northwest. For the first time the core area of the Ouachita fold belt was elevated resulting in the erosion and transportation of chert pebbles and other sediment to the northwest. Beginning in the middle Desmoinesian, deposition was in a narrow successor foreland basin (Molasse Basin) northwest of the Arkoma Basin with the Ouachita fold-thrust belt acting as the primary source for terrigenous sediments for the remainder of the Pennsylvanian (Sutherland, 1988).

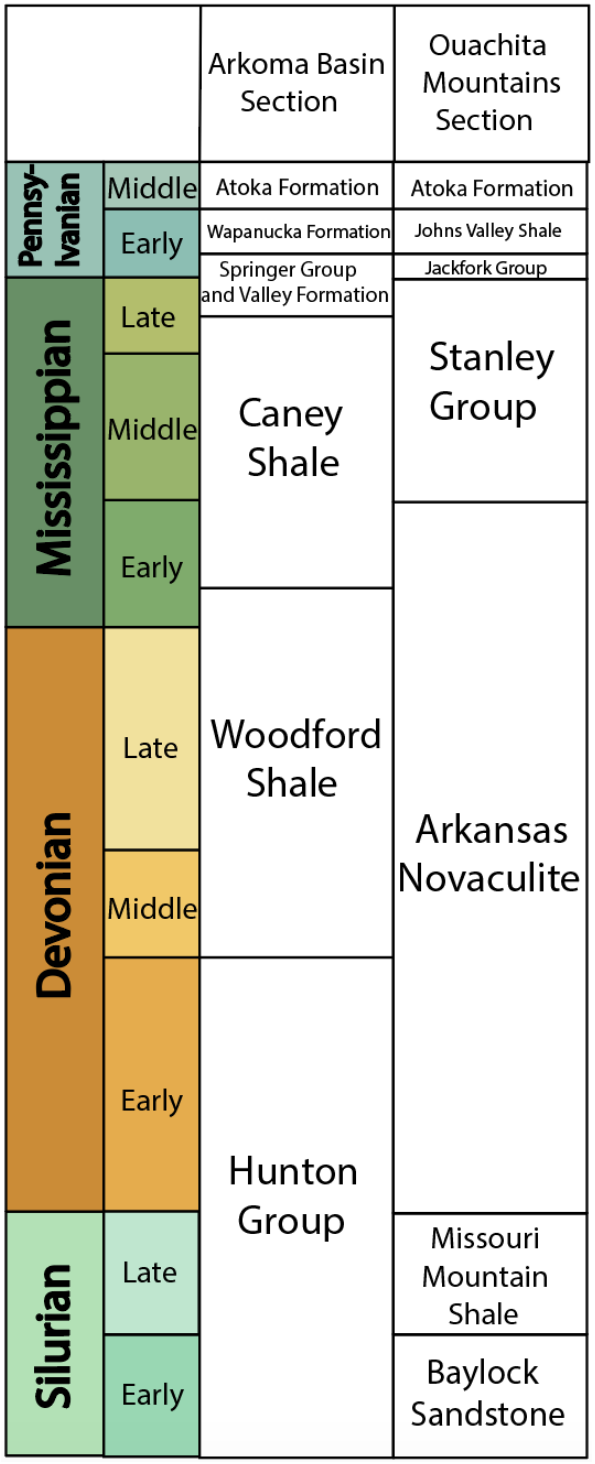

Figure 13-Stratigraphic column of Silurian-Devonian units in the Arkoma Basin and Ouachita Mountains. Within the Ouachita Mountains the stratigraphic-time equivalent of the Woodford is known as the Arkansas Novaculite and is present within the Atoka outcrop.

WOODFORD SHALE

The Woodford Shale is a well-known major source rock in the Midwestern U.S. (Sierra et al., 2010) acting as the most prolific source

rock in the Arkoma Basin and has become a principal target for unconventional oil and gas reservoirs. It was deposited during the late Devonian to early Mississippian (Fig. 13) and consists of black to dark grey, highly organic, marine shale (Cardott, 2012). It unconformably overlies the Hunton limestone, recording the transition from predominantly carbonate deposition into clastic deposition in the later parts of the Paleozoic, and is often subdivided into three informal members referred to as Lower, Middle, and Upper Woodford (Sierra et al., 2010) (Fig. 14). Most of the organic material in the Woodford consists of Type II kerogen but minor amounts of Type III have been identified (Houseknecht et al., 1992; Kirkland et al., 1992). In the Arkoma Basin the Woodford has thermal maturities that favor the production of dry gas, however, some wells on the western and southern margins do produce oil and/or condensate (Suneson, 2012).

The Woodford was deposited in an epeiric sea during a period of anoxia, providing conditions conducive to the preservation of organic material. The organic rich middle member (Fig. 14) has a mean total organic carbon (TOC) of 5.4% but can reach up to 26% TOC in some areas (Spotl et al., 1998). Sea level changes during Woodford deposition are documented on two scales; long term 1st and 2nd order cycles; and short-term 3rd and 4th order cycles (Milad, 2017). The Woodford is generally considered a transgressive succession (Comer, 2005; Comer, 2008) with the depositional setting being interpreted as a west-facing, passive continental margin in an arid climate heavily influenced by marine upwelling (Lowe, 1975; Parrish, 1982, Kirkland et al., 1992; Comer, 2005; Comer, 2008). These conditions favored high organic productivity and the accumulation of highly concentrated organic matter with minimal input of terrigenous clastic sediment (Allen and Allen, 2013; Houseknecht, 2014).

The three informal members (Fig. 14) are related to varying environments of marine deposition and are recognized based on differences in palynology, organic geochemistry, and electric log responses (Cardott, 2012). The lower and middle members generally have an elevated clay content of about 30% (Sierra et al., 2010) and low silica content. Most of the hydrocarbon producing organic material is present in the middle member. The upper member is important for the unconventional reservoirs because it has an elevated silica content, upwards of 80% in some sections (Cardott, 2013), and a low clay content of about 20% (Sierra et al., 2010). This adds a significant brittleness to this member causing it to respond well to hydraulic fracturing as an unconventional gas-shale reservoir.

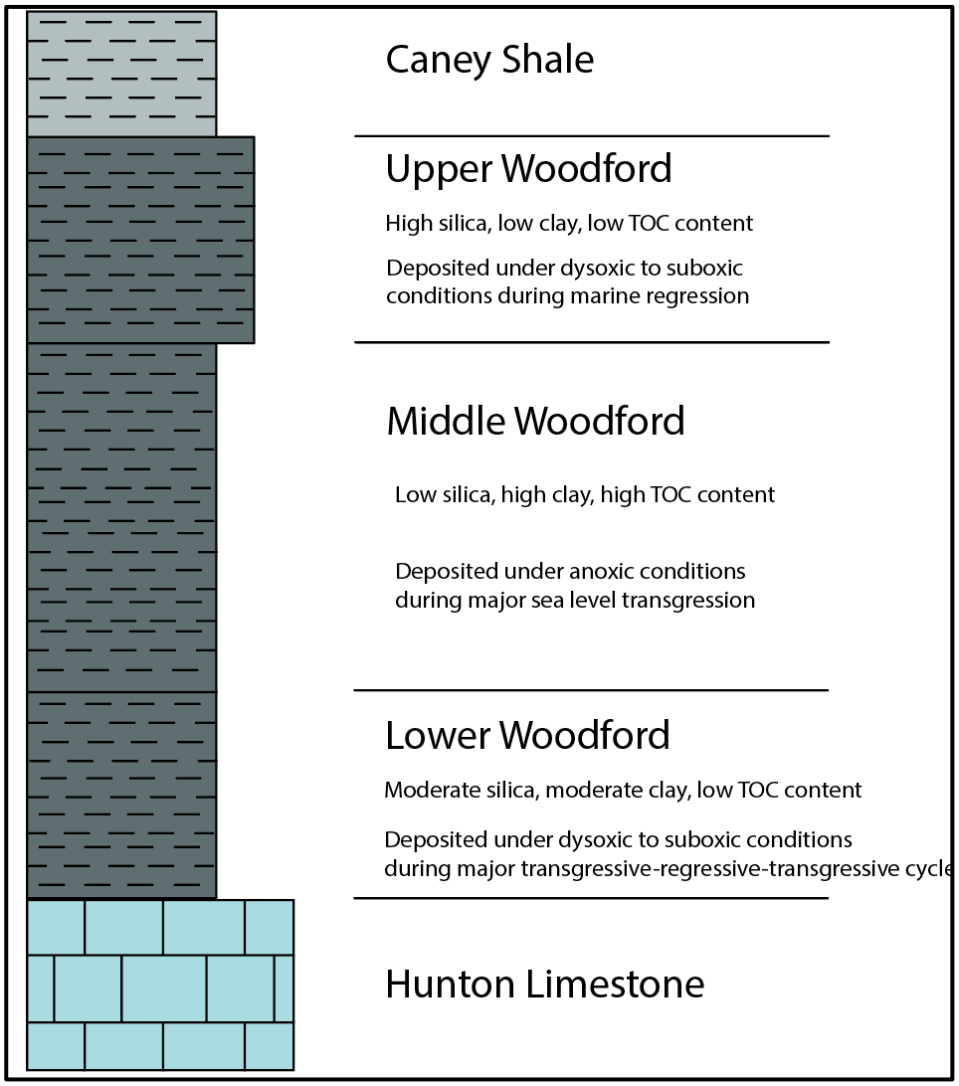

Figure 14- Stratigraphic column of the Woodford Shale's lower, middle and upper members and their respective compositions and depositional environments.

Most of the silica in the upper member that makes it so brittle is biogenic in origin and was derived from Radiolaria and sponge spicules (Cardott, 2012) that were present in its depositional environment. The proportion of chert in the Woodford increases southward toward the deep basin and

continental margin (Houseknecht, 2014). This is because during the late Devonian, the dominant wind and flow direction was directed northwest, causing the southeastern continental margin to be influenced by intense marine upwelling and radiolarian production. During the late Devonian, northern portions of Oklahoma were farther from the continental margin where upwelling was not as intense therefore producing a smaller population of radiolarian (Kvale and Bynum, 2014). These conditions during the late Devonian favored high organic productivity and accumulation of concentrated organic matter as well as an increase in siliceous ooze towards the basin. The basin reflects an increase in water depth which favored the accumulation of greater volumes of the siliceous ooze coming from the high populations of radiolarians living on the continental margin. And this increase in silica can be observed in the increased amount of chert eastward in the Arkansas Novaculite and basinward from the town of Arkoma towards the Ouachita Mountains (Houseknecht et al., 2014).

The Hunton Limestone unconformably underlies the Woodford Shale and has heavily influenced the early stages of deposition in the Woodford. This is due to karsting being a common feature on the unconformable surface separating the two units, causing topographic irregularities. Karst features such as collapses and sinkholes create karst lows where Woodford sediment infilled in the early stages of deposition during the Devonian transgressive cycle over the karstic Hunton surfaces. This led to thicker intervals of Woodford in the karst lows as well as potential “sweet spots” for drilling targets. Inversion of 3D seismic data and gamma ray logs often reveal TOC enriched intervals at or near the basal unconformity (Althoff, 2012) between the Hunton carbonate and Woodford Shale because of the early marine transgression into the topographic depressions that hindered water circulation and gave rise to localized anoxic depositional environments (Slatt et al., 2015).

NATURAL FRACTURES

Fractures represent a mechanical discontinuity and develop due to stress put on a rock unit (Davis et al.,2012). They are found in almost all outcrops of rock but are most prominent in highly competent rocks such as sandstone, limestone, quartzite, and granite (Davis et al., 2012). In sedimentary rocks, lithological factors such as composition, bed thickness, clay type, and porosity play a significant role in fracture development. A sedimentary rock unit that consists of more brittle content such as silica tends to increase bed thickness due to the increased rate of sedimentation. And thick beds tend to have fewer fractures because of their ability to compensate for more stress (Nelson, 1985).

There are three fundamental modes of loading that create stresses which lead to fracture development: Mode I (opening), Mode II (Sliding), and Mode III (Scissoring) (Atkinson, 1987; Engelder, 1985) (Fig. 15). Mode I fractures form by opening due to pure extension (opening) driven by tensile stresses perpendicular to the fracture plane (Younes and Engelder, 1999) and have no shear traction. In contrast, Mode II and III loading creates shear traction parallel to the plane of the fracture surface with no opening. The only difference between Mode II and III loading is the direction of shear traction relative to the propagation direction of a fracture surface (Davis et al., 2012). Mode I loading is the most common producer of fractures networks under tensile stresses.

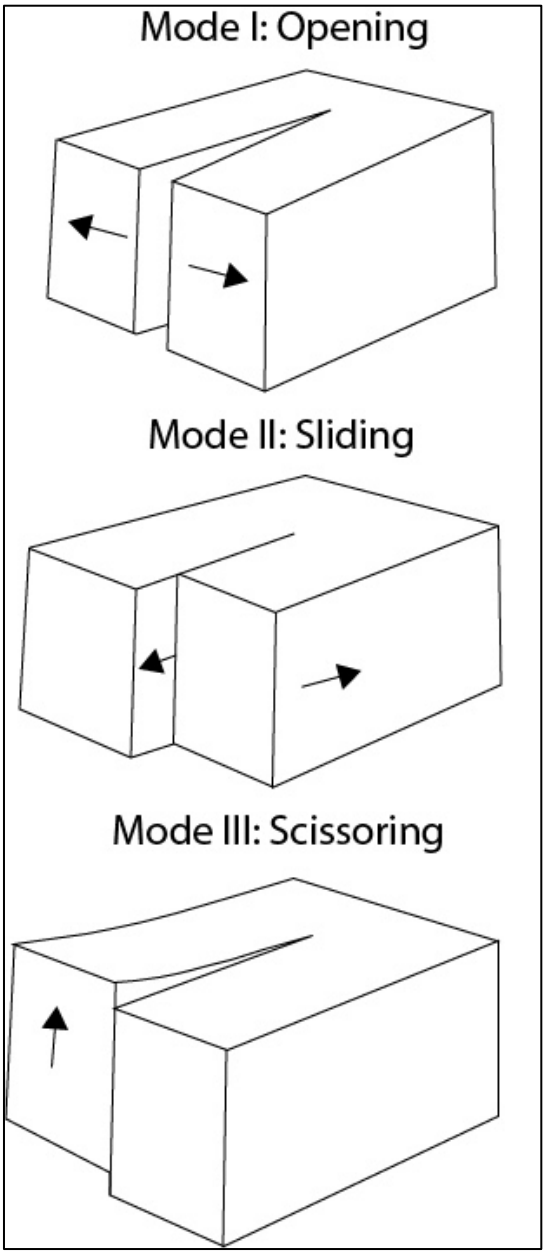

Figure 15- Modes of loading responsible for fracture development. Mode I opening is responsible for most fractures however fractures can still develop from sliding (Mode II) and Scissoring (Mode III) stresses. Fractures may also form from multiple modes of loading known as mixed mode loading (Modified from Engelder, 1985)

Fractures may be characterized as either systematic or nonsystematic (Engelder, 1985). Systematic tensile fractures are characterized by parallel or subparallel orientation and regular spacing and often form parallel to the direction of tectonic compression responsible for folding. In contrast, nonsystematic tensile fractures generally from due to unloading and typically display curved or irregular geometries that do not share a common orientation (Ataman, 2008). Nonsystematic fractures can form at the same time as systematic

fractures, however, if they die out at the intersection of systematic fractures this indicates that the nonsystematic fractures formed later than the systematic fractures (Twiss and Moores, 1992). Barton (2014) states that "no two shales are alike" and proposes nonlinear shear strength in shales and that not all major fracture sets will form parallel to the major principal stress direction due to the effects of shearing. Shear stiffness of shales in situ vary significantly due to shale fabric and stiffness changes, resulting in local rock stress changes. So, a nonlinear model is likely to give a more realistic prediction of gas-shale stimulation performance.

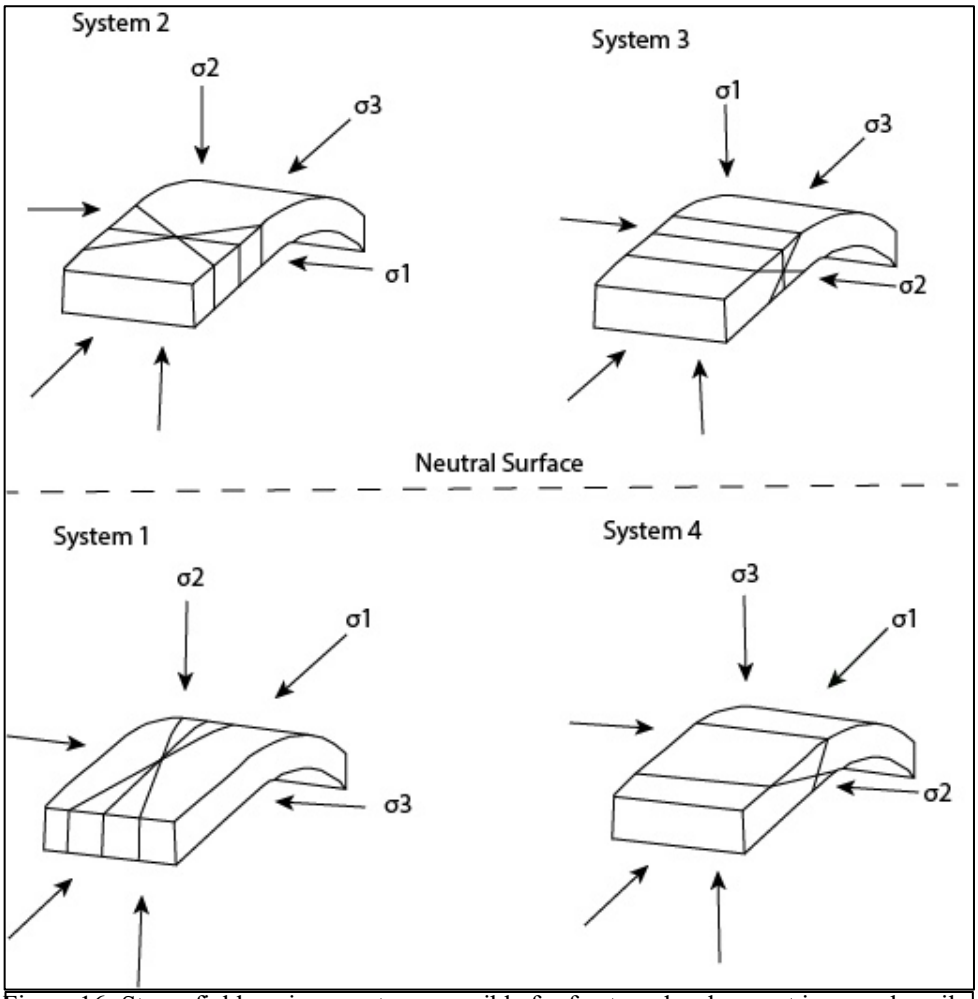

Figure 16- Stress-field environments responsible for fracture development in areas heavily influenced by folding (modified from Engelder, 1985).

Fractures formed due to folding, such as those at the Atoka outcrop, have been the focus of numerous fracture related literature (e.g., Stearns, 1964; Bergbauer and Pollard, 2004). Stearns (1968) created a model of how fractures develop during folding, which was later revised by Bergbauer and Pollard (2004). This model (Fig. 16) proposed that there are four systems that correspond to four distinctive stress-field environments. Systems 1 and 2

(Fig. 16) are marked by conjugate strike slip shear fracture sets and mode I joints. System 3 is composed of conjugate normal shear fracture sets and mode I joints. System 4 is composed of conjugate thrust shear fracture sets and mode I joints.

CHAPTER III

RESULTS

FRACTURE ANALYSIS

The two outcrops that were studied during this study were marked with two 1m inventory squares highlighting areas where the fracture analysis was conducted. The measurements of bedding thickness and fracture spacing during the fracture analysis was done using RIEGL RiSCAN Pro software in order to quantitatively determine if there was a relationship between the fracture spacing and bedding thickness. Once the average fracture spacing in the bed was found the fracture density was calculated by dividing the number of fracture present by the total distance measured which was roughly 100 cm (1m) for every bed. Fracture spacing is simply the amount of space between each fracture and is measured in cm and converted to meters for this study. Fracture density, sometimes referred to as fracture intensity, is the number of fractures present over a given measurement. For this study fracture density was calculated using the number of fractures per cm in one-meter-long beds with varying thicknesses.

a. Wapanucka Outcrop Fracture Analysis

The Wapanucka outcrop is located in the Wapanucka shale pit roughly 2 miles southwest of the town Wapanucka, Oklahoma at 34°20'47.07"N 96°26'4.47"W (Fig. 2). At this location the outcrop consists of gently dipping Woodford Shale and gives off a hydrocarbon odor whenever samples are broken. It contains phosphate nodules and pyrite indicating it is part of the silica rich upper Woodford member (Cardott, 2007; Mnich, 2009; Portas, 2009; Portas and Slatt, 2010; Slatt et al., 2011; Hanzel, 2012; Cardott, 2012; Milad and Slatt, 2017). The beds strike N55°W and dip 22° NE. There are two systematic fracture networks present. The first set trends N15°W and the second set trends roughly N80°E, both fracture networks are vertical. The outcrop was marked with two inventory squares in order to study the natural fracture patterns which are referred to as Wapanucka – 1 and Wapanucka – 2 (Fig. 17).

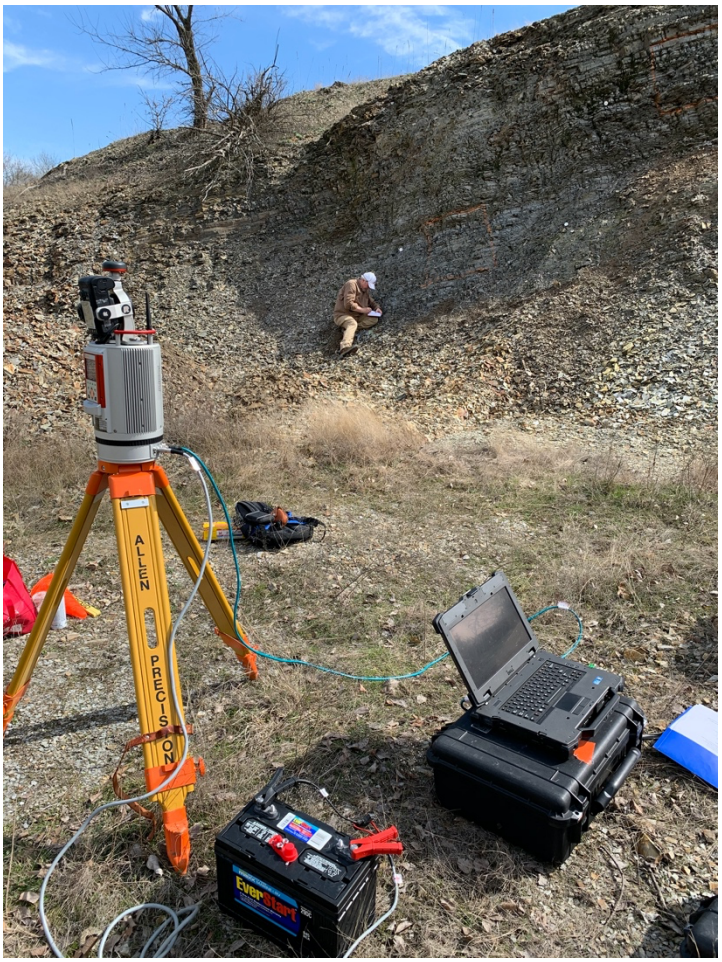

Figure 17a – Field measurements being taken at the Wapanucka outcrop with the use of LiDAR

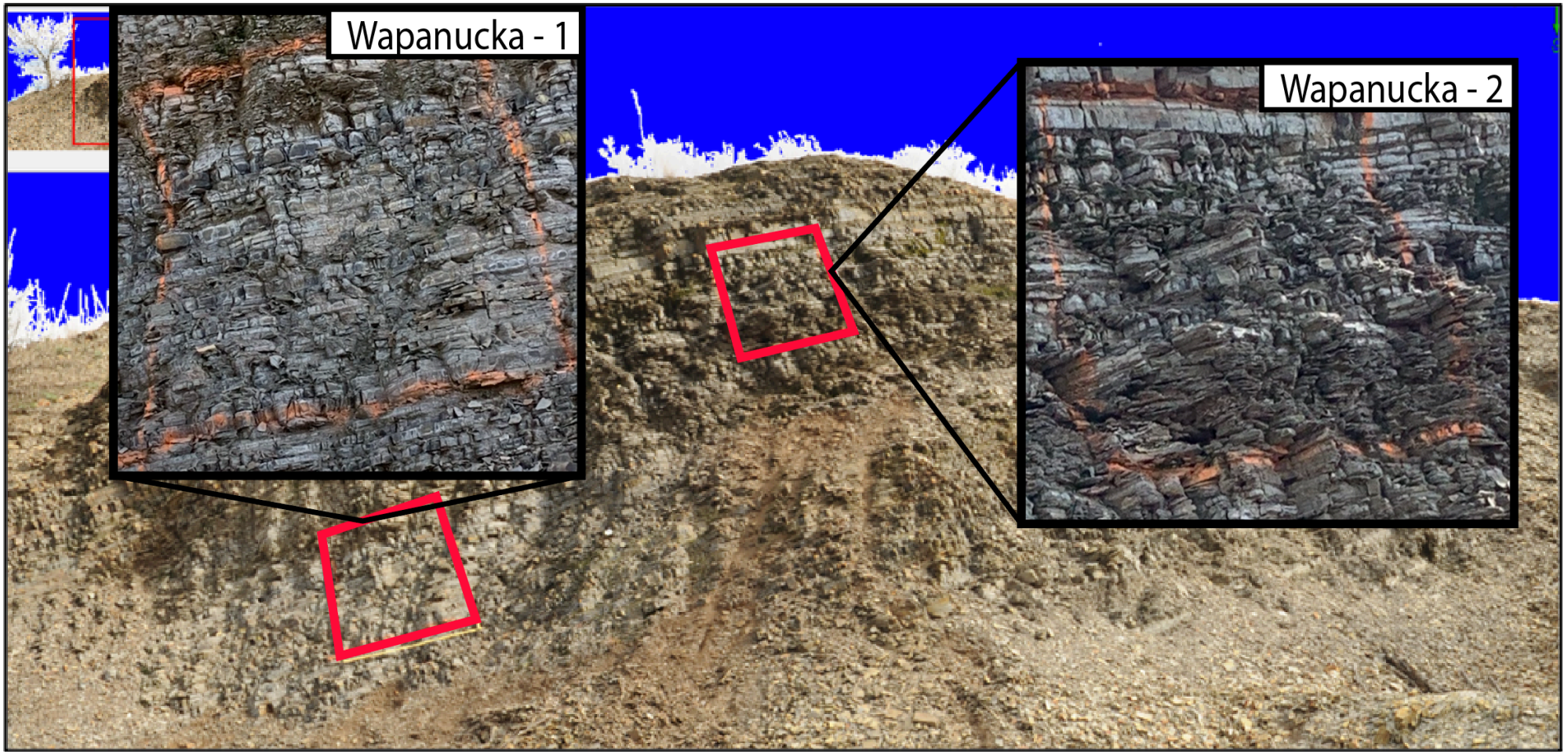

Figure 17b- Highlighted inventory squares at the Wapanucka outcrop. Inventory squares have been enhanced in order to more accurately show the beds and fractures present that were measured for the fracture analysis. Inventory squares are named Wapanucka – 1 and Wapanucka – 2 in order to differentiate the two.

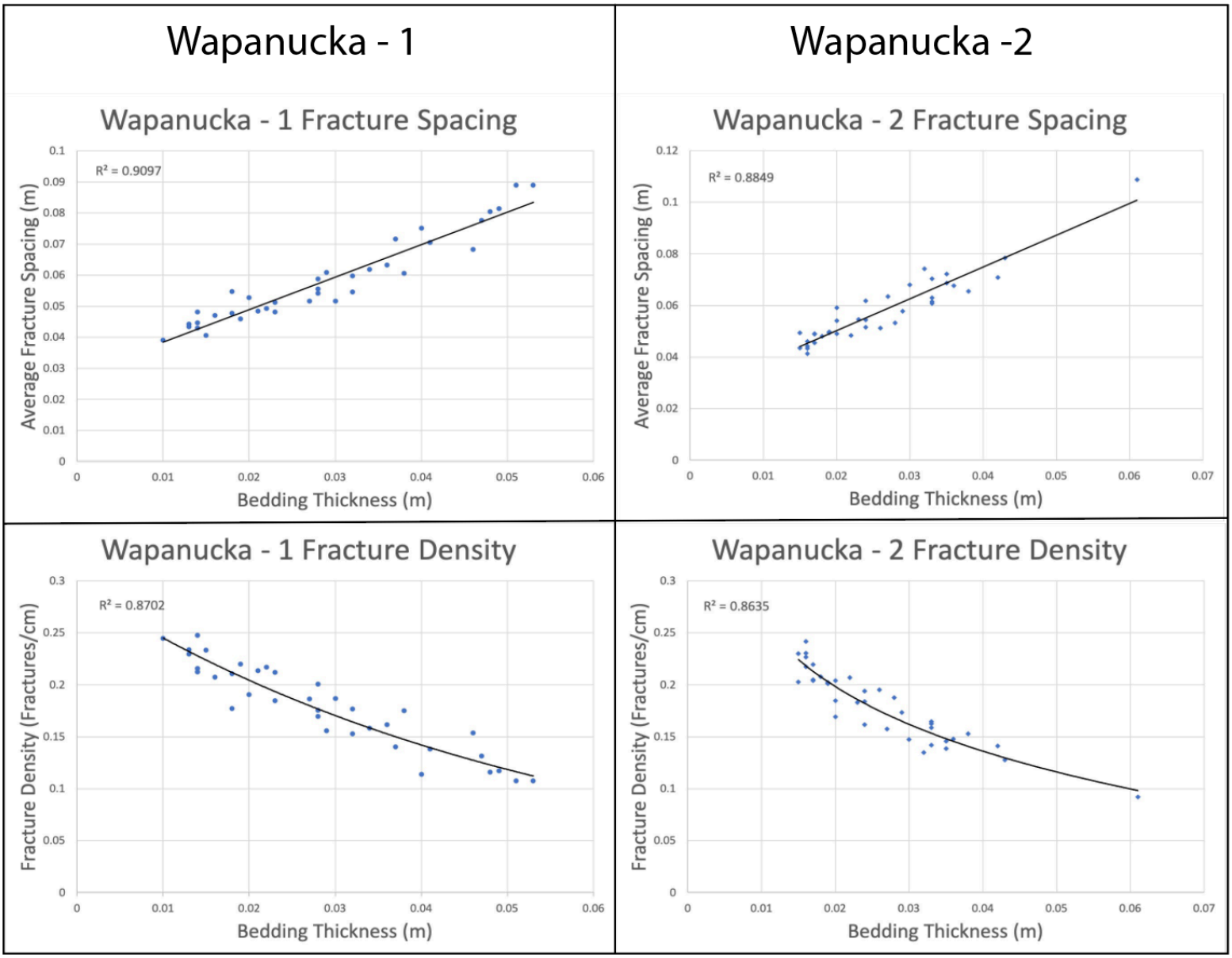

Figure 18- Results of the fracture analysis within the two inventory squares at the Wapanucka outcrop. These results show a direct relationship between bedding thickness and fracture spacing as well as bedding thickness and fracture density. As bedding thickness increases fracture spacing will increase as well, and as bedding thickness increases bedding thickness will decrease.

Using RiSCAN Pro to measure the bedding thicknesses and fracture spacings within the inventory squares, a strong relationship between the two parameters was established (Fig. 18). As the bedding thickness increases the fracture spacings increase as well. With this information a relationship between bedding thickness and fracture density was also established, however this

relationship is inverse compared to fracture spacing. As bedding thickness increases fracture density will decrease, or in other words, higher concentrations of fractures are found in thinner beds. The two inventory squares have R^2 values around 0.90 for both the fracture spacings and fracture densities which indicates that this relationship remains strong as long as the Woodford contains homogenous material, free from any defects such as fossils, and has not undergone any significant deformation.

The statistical analysis for the relationships between bedding thickness, fracture spacing, and fracture density were established using Microsoft Excel. For fractures spacing, the spacings between all fractures in a given bed were measured and then averaged to obtain an average fracture spacing. This average fracture spacing was plotted on a graph against the thickness of the bed. Once every bed had been plotted a line of best fit was added in order to assess the strength of the relationship. Fracture density was then calculated by dividing the number of fractures present over a given length. This fracture density was also plotted against the thickness of the bed and then overlain with a line of best fit to observe the strength of the relationship. The high R^2 value for all Wapanucka graphs indicates that there is a strong relationship between the thickness of the bed and its fracture characteristics. Although some literature has argued that Excel contains poor algorithms that may lead to incorrect results when calculating large data sets such as the one in this study (McCullough, 2005; Knusel, 2005). Others, however, argue that these statistical bugs are trivial and are not a major source of misrepresentation of any data (Pace, 2008; Melard, 2014). Therefore, the statistical analysis run in Excel is appropriate and conclusive for this study.

b. Atoka Outcrop Fracture Analysis

The Atoka outcrop is located 1.5 miles southeast of the town of Atoka, Oklahoma (Fig. 3). The outcrops coordinates are 34 22'31.63" N and 96 06'35.77" W. This outcrop is unique in the sense that it consists of the Arkansas Novaculite, which is a time-stratigraphic equivalent to the Woodford Shale located in the Ouachita Mountains. It is located close to the southern boundary of the Arkoma Basin; the frontal Ouachita fault zone, also named the Choctaw Fault Zone. The fault zone has caused the outcrop to be heavily deformed and Woodford beds are steeply dipping with superimposed folding (Fig. 19). This provides a unique opportunity to observe how fractures are affected in areas of significant deformation. The beds at this outcrop strike roughly N40°E and dip 68° NW, however, the heavy deformation causes the strike and dip to be quite variable and can change up to 15° in less than a few hundred meters (Ataman, 2008). There outcrop contains two systematic fracture sets; the first set trends N35E and the second trends N60W. Similar to the Wapanucka fracture networks, both networks here are vertical. The Atoka outcrop was also marked with two 1m inventory squares which are referred to as Atoka – 1 and Atoka – 2.

The natural fracture patterns at the Atoka outcrop exhibited a similar relationship between bedding thickness, fracture spacing, and fracture density as the Wapanucka outcrop (Fig. 20). As bedding thickness increases, fracture spacing increases, and fracture density decreases. However, the Atoka – 1 inventory square does not show as strong of a relationship as the Atoka -2 inventory square and both inventory squares at the Wapanucka outcrop. The relationship

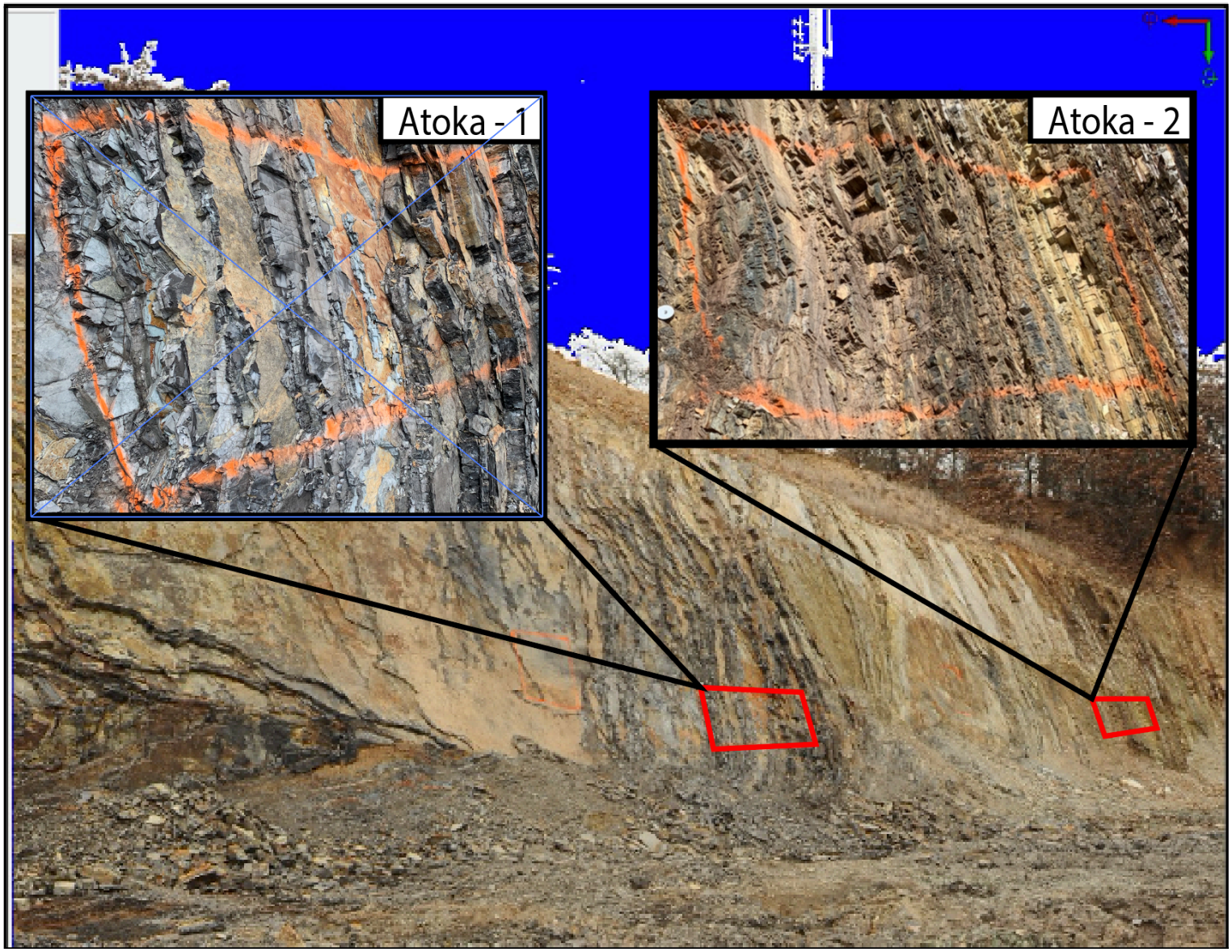

Figure 19- Highlighted inventory squares at the Atoka outcrop. Squares have been enhanced in order to show the beds and fractures that were measured in both inventory squares. Naming of these squares follows the same method as the Wapanucka outcrop naming these two Atoka – 1 and Atoka – 2 respectively.

between fracture spacing and bedding thickness at Atoka – 1 has an R^2 value of 0.74 and for fracture density 0.70. These unfavorable R^2 values indicate that the relationship is not as consistent and the intense deformation has created more complex fracture networks that are not present in the other inventory squares.

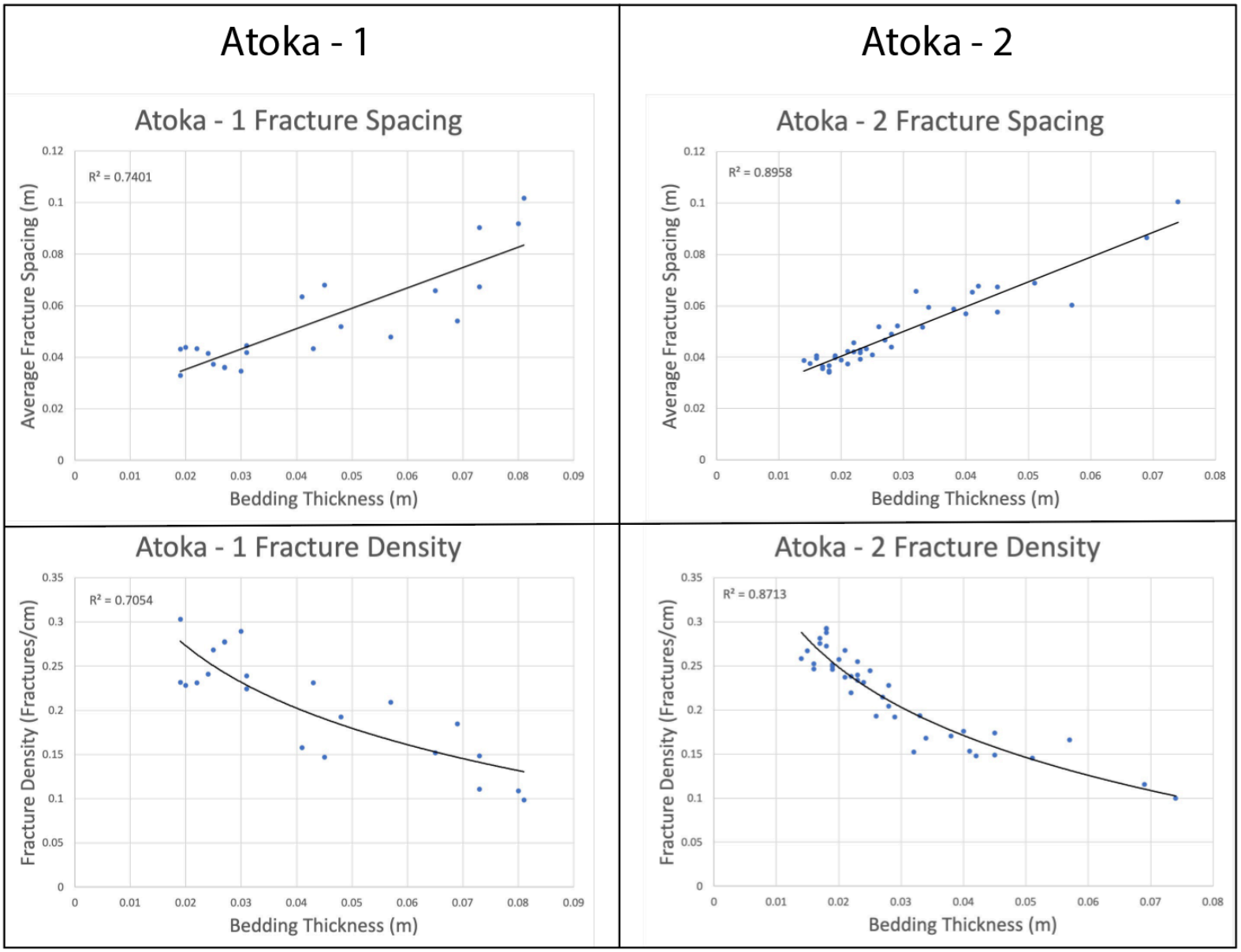

Figure 20- Results of the fracture analysis at the Atoka outcrop. The relationship between bedding thickness, fracture spacing, and fracture density remains consistent at the Atoka outcrop. However, the Atoka - 1 inventory square has a lower unfavorable R^2 value indicating more complex fracture networks are present in this section of the outcrop. These complex networks are likely a result of increase bedding thickness which is indicative of increased silica content which responded to the intense deformation in the outcrop in a brittle manner.

However, at the Atoka – 2 inventory square, there is a strong relationship between bedding thickness, fracture spacing, and fracture density similar to the fractures at the Wapanucka outcrop. The R^2 values for the relationships at Atoka – 2 are 0.89 for fracture spacing and 0.87 for fracture density. This indicates that there is a unique property causing the Atoka – 1 inventory square to fracture in a much less consistent way than all other inventory squares measured. This can likely be explained by the average bed thickness in the Atoka – 1 inventory square being 0.043m (4.3 cm) compared to only 0.029m (2.9 cm) at Atoka – 2, 0.026m (2.6 cm) at Wapanucka – 2, and 0.028m (2.8 cm) at Wapanucka – 1. A larger average bedding thickness in Atoka - 1 is indicative of an elevated silica content in this area of the outcrop and beds with an elevated silica content tend to fracture in a more brittle manner (Nelson, 1985). This means Atoka – 1 likely responded to the intense deformation much differently than Atoka – 1, which has a much lower average bedding thickness.

The relationships between bedding thickness, fracture spacing, and fracture density for the Atoka inventory squares were calculated using the same methods as the Wapanucka squares. Meaning the shortcomings of using Microsoft Excel that were previously outlined could potentially have an effect on the unfavorable R^2 value seen within the Atoka – 1 inventory square.

PETROGRAPHIC ANALYSIS

A petrographic analysis was conducted using polished thin sections of selected samples to assess the silica content in different stratigraphic levels and bedding thicknesses within each outcrop. Thin sections were created from five different samples at the Atoka outcrop and three from the Wapanucka outcrop. Bedding thicknesses of these samples ranged from 1” – 3” to

examine if the silica content varied in the different bed thicknesses. The amount of silica present was estimated based off of visual observation, more accurate weight percentages of silica are obtained from XRF analysis. Silica content within the Woodford increases to the southeast which is apparent when looking at the average bedding thicknesses of the inventory squares at each outcrop. Atoka – 1 had a significantly higher average bedding thickness when compared to all other inventory squares, which is an indicator of increased silica.

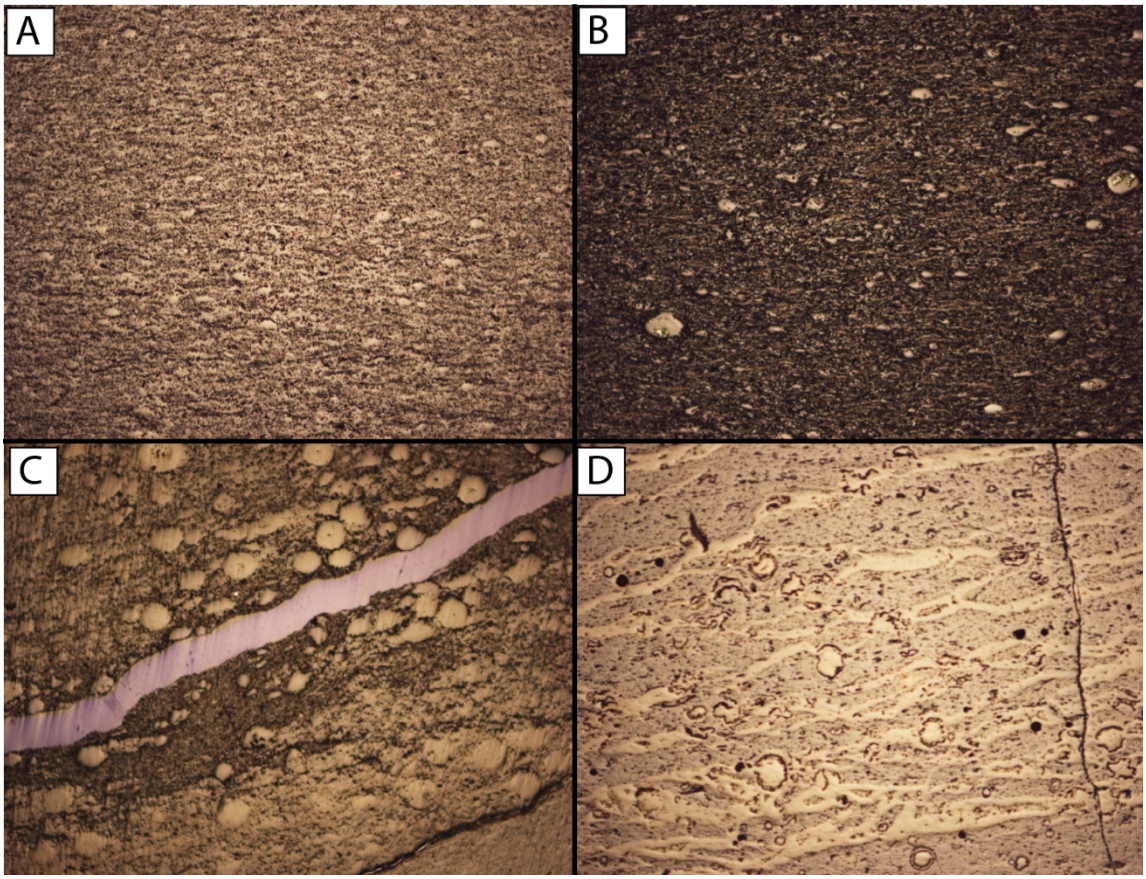

Figure 21- Thin sections at 4x magnification of Woodford Shale and Arkansas Novaculite at varying bed thicknesses (A) 3" bed of Woodford Shale from Wapanucka outcrop. (B) 1" bed of Woodford Shale from the Wapanucka outcrop. (C) 2" Bed of Arkansas novaculite at the Atoka outcrop. (D) 1” bed of Arkansas Novaculite from the Atoka outcrop.

In thin section view pyrite and small amounts of bitumen are present which indicate that these outcrops are part of the upper Woodford member. The thin sections were also observed in order to determine the source of the silica Most of the silica content is in the form of radiolarians

(Fig. 21) indicating biogenic origin. Some of the radiolarians have also been replaced with pyrite (Fig. 10). When looking at the quantity of silica present it is apparent that there is in fact a correlation between bedding thickness and silica content. Thin sections that were prepared from beds of ~3" had significantly more radiolarian nodules and silica than beds of approximately 1" in thickness. Interestingly, samples taken from 3" thick beds in the Atoka – 1 inventory square did not appear to be as abundant in biogenic silica, however, the samples appeared to be almost pure silica.

XRF DATA

X-Ray Fluorescence (XRF) data was obtained in order to assess the weight % of silica in different bedding thicknesses. Five samples from the Atoka outcrop and four samples from the Wapanucka outcrop with bedding thicknesses ranging from thinly laminated to 2" were prepared into glass beads and sent to Pomona College in California for XRF analysis. This method allowed for the thinly laminated samples to be analyzed for their geochemical properties, which was not able to be done with thin sections. This method also allows for the precise weight % of silica present in each bed which is more useful than estimates found in the petrographic analysis. However, the petrographic analysis allows for the characterization of the silica type, which in this case, is biogenic.

Fig. 22 shows the XRF results for all 9 Woodford samples, most notably silica content, and fig. 23 graphs the silica content against bedding thickness for each sample. These results show that generally the higher the silica content is the thicker the bed will be. This can then be

Sample	A-1-1	A-2-1	A-3-1	A-4-1	A-6-1	W-1-1	W-2-1	W-4-1	W-5-1
SiO2	94.65	94.78	95.49	81.57	93.67	90.44	79.68	73.14	94.56
TiO2	0.08	0.07	0.04	0.42	0.12	0.25	0.54	0.43	0.11
Al2O3	2.24	1.66	1.03	8.61	2.62	4.68	10.56	8.60	2.27
Fe2O3	2.24	2.76	3.00	5.33	2.15	2.21	4.02	3.73	1.75
MnO	0.01	0.02	0.02	0.07	0.01	0.01	0.01	0.01	0.01
MgO	0.18	0.12	0.06	0.87	0.20	0.37	0.90	0.74	0.17
CaO	0.04	0.04	0.03	0.06	0.15	0.29	0.23	5.63	0.31
Na2O	0.00	0.00	0.00	0.09	0.00	0.13	0.10	0.06	0.03
K2O	0.47	0.37	0.20	2.01	0.58	1.21	3.14	2.58	0.54
P2O5	0.03	0.07	0.05	0.74	0.31	0.23	0.31	4.49	0.11
Total:	99.94	99.90	99.93	99.78	99.82	99.81	99.49	99.41	99.84

Figure 22- XRF results for all 9 samples. Silica content ranges from 73.14% up to 95.49%. Samples A-1-1, A-2-1, and A-3-1 were taken near Atoka – 1 inventory square where additional complex networks are present. A-4-1 and A-6-1 are from near the Atoka – 2 inventory square. W-1-1, W-2-1, A-4-1, and W-5-1 samples taken from the Wapanucka outcrop.

related to the relationship previously established between bedding thickness, fracture spacing and fracture density. Thicker beds with a higher silica content will have a lower fracture density and generally develop fractures farther spaced apart. And the thinner, lower silica beds, will have an increased fracture density developing fractures more closely spaced together.

When looking at the silica content for the Atoka outcrop, the three samples that were taken from near the Atoka – 1 inventory square (A-1-1, A-2-1, A-3-1) where the bedding thickness and fracture relationship was less favorable, the silica content is extremely elevated upwards of 96% (Fig. 22). This compared to the samples taken

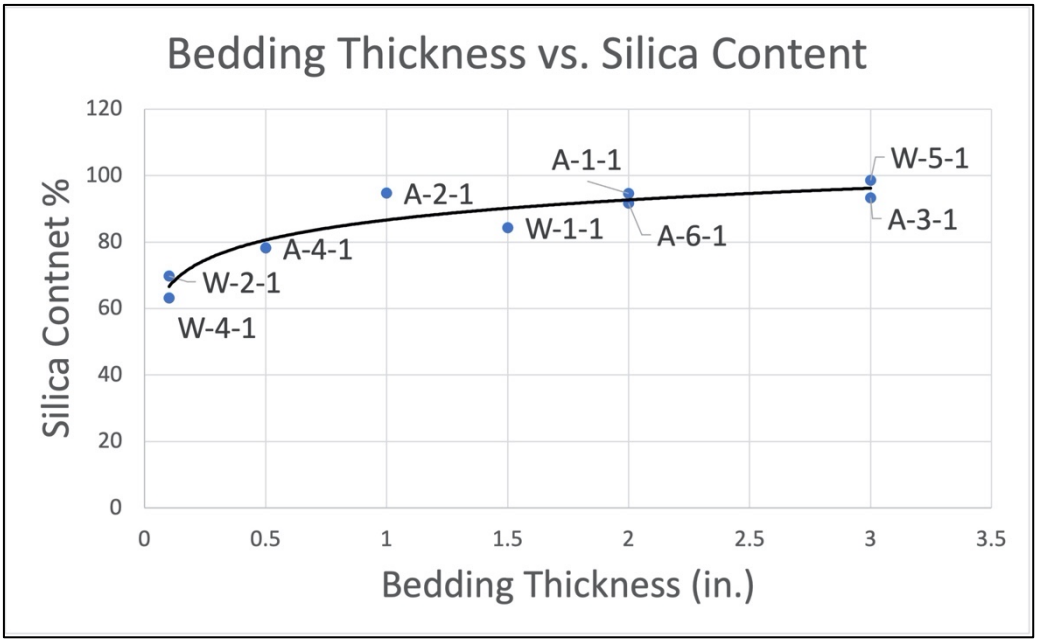

Figure 23 – Silica content of each sample plotted against bedding thickness. This shows that generally as bedding thickness increases so will the silica content.

near the Atoka – 2 inventory square (A-4-1, A-6-1), and all Wapanucka samples, where the bedding thickness-fracture relationship was more favorable, the silica content is generally lower. This indicates that the complexity of the fracture networks near the Atoka – 1 inventory square are potentially due to the elevated silica content in this section of the outcrop, causing the relationship between bedding thickness and fracture characteristics to be weaker than all other inventory squares.

COMPARATIVE ANALYSIS

Other Devonian shale fracture studies done in southeastern Oklahoma and northeastern Alabama are compared to the results of this study in order to assess the regional significance of the fracture networks in the Atoka and Wapanucka outcrops. Clark (2015) used terrestrial LiDAR to study fracture spacings and fracture densities in outcrops of Chattanooga Shale in northeastern Alabama. Clark's results reinforce the relationship between bedding thickness, fracture spacing, and fracture density observed in the Woodford Shale. The two outcrops in Clark's study exhibited an increase in fracture spacing as bedding thickness increases and a decrease in fracture densities as bedding thickness increases. The Chattanooga Shale shares similar characteristics to the Woodford Shale having a silica rich upper member that favors fracturing in a brittle manner, making it a good analogue for quantitatively analyzing natural fractures.

Hanzel (2012) used terrestrial LiDAR to image the Woodford Shale in the McAlister Shale Pit located 8 miles south of Ardmore Oklahoma, roughly 60 miles southwest of the Wapanucka outcrop (Fig. 23) where a complete section of the Woodford Shale is exposed. Hanzel (2012) studied all members of the Woodford, but only the upper Woodford is compared to the Wapanucka outcrop. The upper Woodford is striking N29°W and dipping 37°NE with three fracture sets identified. The first set of fractures (Set A) trends N30°E, the second (Set B) N20°W, and the third (Set C) N72°E. The Wapanucka outcrop shares similar structural characteristics striking N55W and dipping 22NE with two fracture networks present that trend N80E and N15W. Meaning the Set B and Set C fractures measured in the McAlister Shale Pit are also observed in the Wapanucka outcrop, however the Set A fractures are not

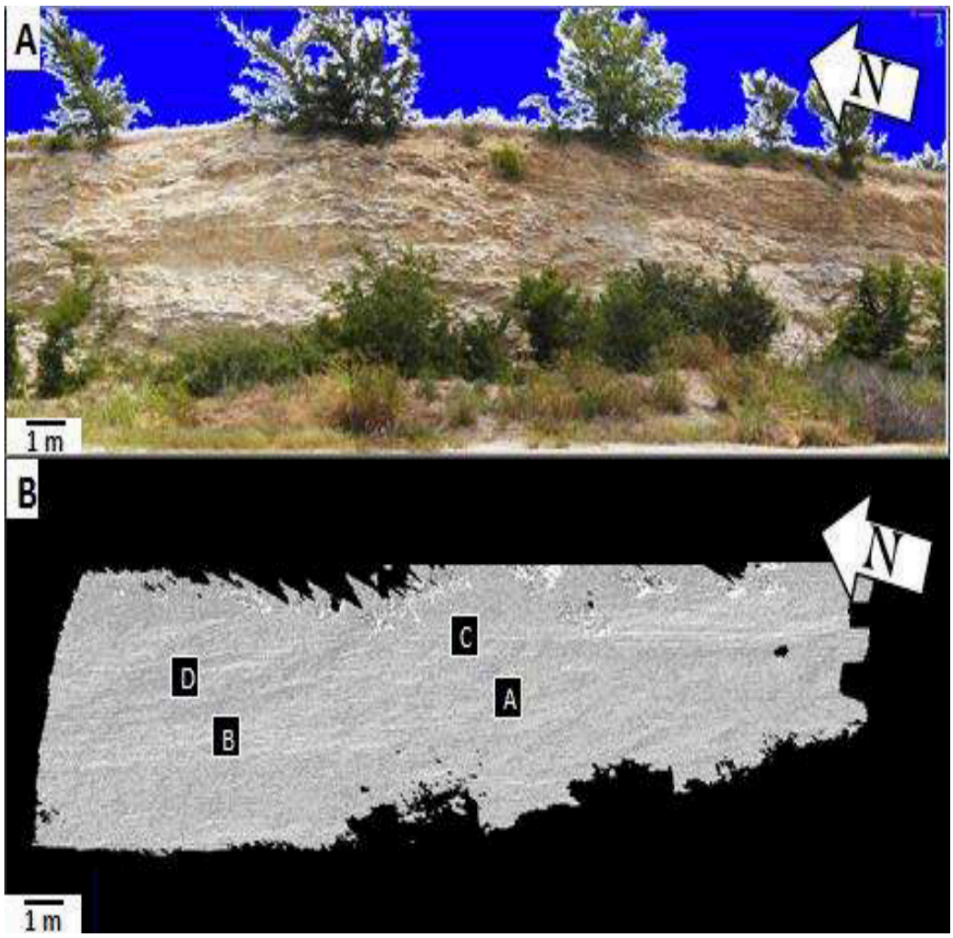

Figure 24- Upper Woodford section measured by Hanzel (2012) at the McAlister Shale Pit, OK. (A) High resolution LiDAR image of the upper section of the Woodford. (B) Fracture networks present within the upper Woodford at this location (D is interpreted as the bed plane).

present in the Wapanucka outcrop. This indicates that the Woodford in the McAlister Shale Pit may have undergone additional deformation that was not experienced in the Wapanucka outcrop.

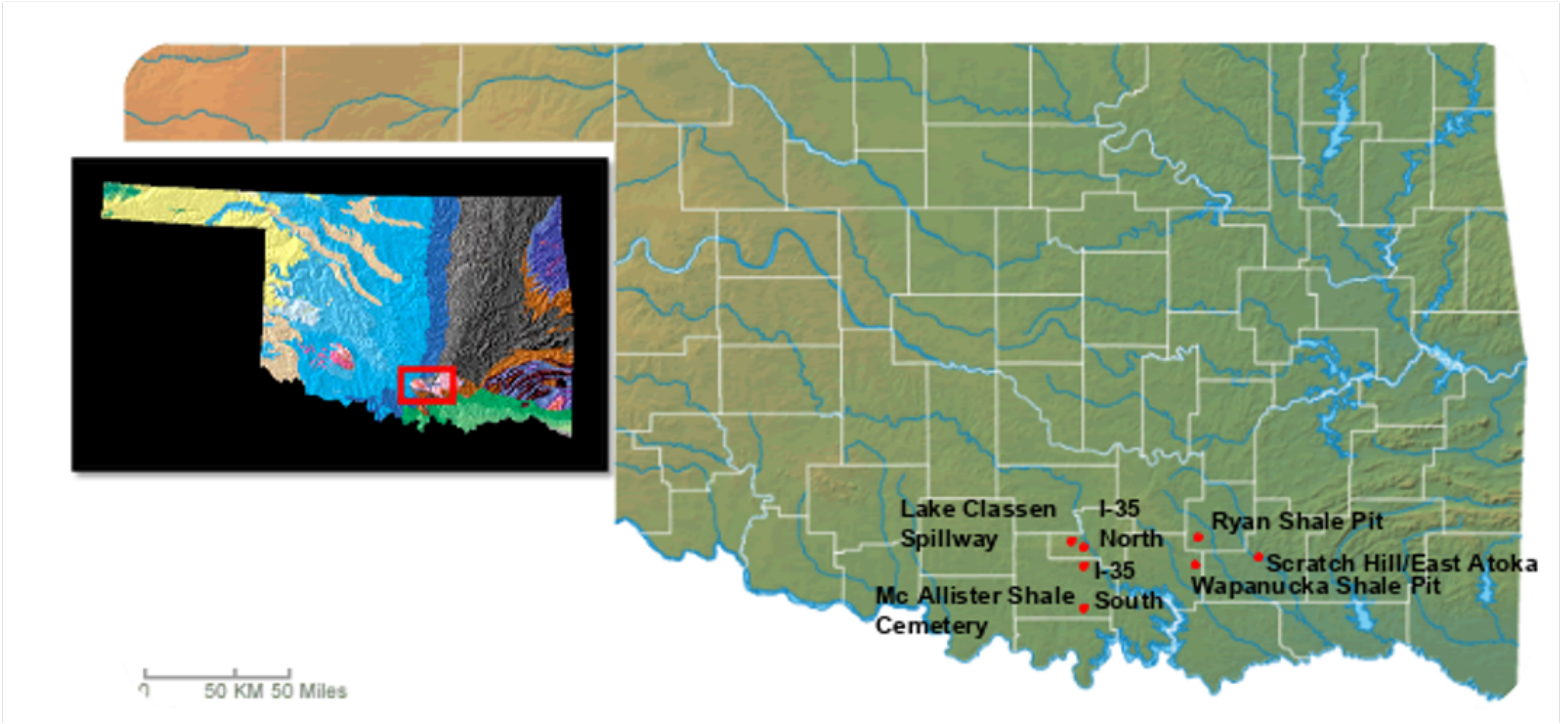

Figure 25- Locations of other Woodford Shale studies conducted in southeastern Oklahoma. Hanzel (2012) studied the McAlister Shale pit. Ataman (2008) studied all outcrops shown here but did not use terrestrial LiDAR and focused on the structural and lithological impacts on fracture formation. Ginter (in prep) studied the I-35 North and I-35 South outcrops, however these results are still being processed. Not imaged here are the Chattanooga Shale outcrops studied by Clark (2015) in northeastern Alabama.

Ataman (2008) studied fracture geometries from multiple outcrops throughout southeastern Oklahoma, including the Atoka and Wapanucka outcrops. However, Atman did not utilize terrestrial LiDAR and was focused on determining the effect of structural and lithological controls on natural fracture development. Other Woodford outcrops studied by Ataman include Lake Classen Spillway, I-35N, I-35S, and the Clarita Shale Pit (Fig. 24). All the outcrops in this study also verify the relationship between bedding thickness, fracture spacing, and fracture density in a rough non-quantitative way of classic measurement with a ruler. This method has

measurement bias and measurement errors. The fracture measurement with LiDAR is precise and overcomes the pitfall of the measurement with a ruler. Fracture networks at the Lake Classen Spillway, I-35N, and I-35S outcrops are difficult to compare to the Wapanucka outcrop as they are primarily fold related. However, the Clarita Shale Pit has gently dipping beds that strike N15°E and has two fracture networks trending E-W and N25°E. These measurements are similar to the Wapanucka outcrop; however, the slight difference could potentially be due to the change in the strike of the beds (Ataman, 2008).

CHAPTER IV

CONCLUSIONS

DISCUSSION

Terrestrial LiDAR has proved its usefulness in outcrop scale natural fracture studies because it accurately measures fracture spacings and bedding thicknesses within millimeters of precision. The use of LiDAR provides many benefits including the ability to study parts of an outcrop that would otherwise be inaccessible to make measurements, reducing uncertainties in measurements by providing precise, high resolution images of outcrop scale natural fractures, and digitizing outcrops for future analysis.

At both the Atoka and Wapanucka outcrops, there is a strong relationship between bedding thickness and fracture spacing as well as bedding thickness and fracture density. As bedding thickness increases, fracture spacing will increase and fracture density will decrease. However, this relationship is not as strong in the Atoka – 1 inventory square where beds are on average significantly thicker generally have a much higher silica content than the beds in all other inventory squares. These two factors likely caused this measured section of the outcrop to respond to the deformation in a more brittle manner, creating additional complex natural fractures that are not present in other sections of the outcrop. While the three other inventory squares having a much lower average bedding thickness and silica content likely caused them to react more ductile to deformation (Nelson, 1985). Therefore, the natural fracture networks

present in the Atoka outcrop may need additional study to fully understand such as differentiating systematic and nonsystematic fractures in order to more accurately model subsurface networks.

The petrographic analysis of varying bed sizes supports the XRF data in showing that thicker beds generally have a higher silica content, although this is highly dependent on depositional environments. The increase in bed thickness in beds with higher silica may be due to the increased sedimentation rate from the biogenic silica. This can also be observed in deep marine environments where high silica chert beds are thinly laminated due to low sedimentation rates. Because of this, the relationship between the silica content and bedding thickness is not linear which is apparent when looking at fig. 23. This analysis also shows that the silica in the upper Woodford is mostly biogenic in origin coming from radiolarians, some of which have been replaced with pyrite (Fig. 10). The petrographic analysis also revealed minor amounts of organic matter such as bitumen even within the thickest, most silica abundant, beds.

The relationship between bedding thickness, fracture spacing, and fracture density remains consistent within the Woodford throughout Oklahoma, as well as in the analogous Chattanooga Shale. Hanzel (2012) and Ataman (2008) observed this relationship to be true for other Woodford outcrops in southeastern Oklahoma and Clark (2015) reinforced this relationship by observing it in the Chattanooga Shale in northeastern Alabama. However, the orientations and geometries of the natural fracture networks varies significantly depending on local structures and lithology of the rock unit controlled by facies variations during the deposition of the sedimentary rock unit. The fracture networks identified in the Wapanucka outcrop were relatable to the fracture networks of Hanzel (2012) measured in the McAlister Shale pit using LiDAR images. However, Hanzel did identify one fracture set that was not present in the Wapanucka outcrop.

Ataman (2008) conducted fracture measurements measured in several outcrops in southeastern Oklahoma. He used a ruler to make his measurements therefore his measurements contain large measurement bias and statistical error. The I-35N, I-35S, and Lake Classen Spillway outcrops Ataman (2008) measured were heavily influenced by localized deformation and did not relate to the fracture networks found in the Atoka or Wapanucka outcrops. This indicates that areas of Woodford Shale that have undergone significant deformation will have unique localized fracture networks that would need additional studies to understand their geometry and mechanical origin, which is the case for the heavily deformed Atoka outcrop.

CONCLUSIONS

This study has determined that Terrestrial LiDAR is a useful tool for quantitatively analyzing natural fractures at the outcrop scale by providing high resolution images that decrease uncertainties introduced by measurement errors, allowing highly quantitative analysis. In a statistically homogenous body of rock free from defects, a linear relationship can be established between bedding thickness, fracture spacing, and fracture density. This relationship shows that fracture spacing increases and fracture density decreases as bedding thickness increases. This relationship remains linear in a statistically homogenous body of rock but will be influenced by the changes in the mineralogy of the rock, such as the amount of silica present in the bed, as well as any local deformation that has acted on the unit.

During this study, a general relationship between silica content, bedding thickness, and fracture density has been determined. Generally, the higher the silica content in a bed the thicker it will be, causing natural fractures to form in a brittle manner increasing the spacing between each fracture, ultimately reducing the fracture density. However, the lower the silica content, and

the higher the clay content, the thinner and more ductile the bed will be. This causes fractures to form closer together, increasing the fracture density. This remains true when the unit is free from intense deformation. When intense deformation acts upon the unit, such as in the Atoka outcrop, additional complex natural fracture networks develop that are characterized by the local stress field acting upon them due to folding and faulting.

REFERENCES

Adams, E.W., Bellian, J.A., Reyes, R., 2009, Digital outcrop models reduce uncertainty and improve reservoir characterization, World Oil, 230(9), pp. 46-49

Ahmadzamri, A.F., Al-Mannai, A.S., Strohmenger, C.J., Foeken, J.P.T., 2014, Virtual Outcrop Geology – A Case Study on Effective Learning and Data Preservation, International Petroleum Technology Conference, January 2014, IPTC 17426

Allen, P.A.; Homewood, Peter; and Williams, G.D., 1986, Foreland basins: an introduction, in Allen, P.A.; and Homewood, Peter, eds., Foreland basins: Blackwood Scientific Publications, Boston, Massachusetts, p. 3-12

Althoff, C. D., 2012, Characterization of depositional megacycles in the Woodford trough of Central Oklahoma, (Master's Thesis): The University of Oklahoma

Ataman, O., 2008, Natural Fracture Systems in the Woodford Shale, Arbuckle Mountains, Oklahoma, (Master's Thesis): Oklahoma State University

Atkinson, B. K., 1987, Introduction to fracture mechanics and its geophysical applications: *in* Atkinson (ed), Fracture Mechanics of Rock: Academic Press, London, p. 1-26

Bellian, J.A., Jennette, D.C., Kerans, C., Gibeaut, J., Andrews, J., Yssldyk, B., and Larue, D., 2002, 3- Dimensional digital outcrop data collection and analysis using eye-safe laser (LIDAR) technology: American Association of Petroleum Geologists (AAPG) Search and Discovery Article 40056,

Bergbauer, S., and Pollard, D., 2004, A new conceptual fold-fracture model including pre folding joints, based on the Emigrant Gap anticline, Wyoming: Geological Society of America Bulletin, v. 116, no. ¾, p. 294-307

Blum, P., R. Mackay, M. S. Riley, and J. L. Knight, 2005, Performance assessment of a nuclear waste repository: Upscaling coupled hydromechanical properties for far-field transport analysis: Journal of Rock Mechanics and Mining Sciences, v. 42, p. 781–792

Blum, P., R. Mackay, and M. S. Riley, 2007, Coupled hydromechanical modelling of flow in fractured rock, in J. M. Sharp and J. Krasny, eds., Groundwater in fractured rocks: International Association of Hydrogeologists Selected Paper Series 9, p. 567–574

Blum, P., Mackay, R., Riley, M. S., 2009, Stochastic simulations of regional scale advective transport in fractured rock masses using block upscaled hydromechanical rock property data: *Journal of Hydrology,* v. 369, p. 318-325

Bour, O., P. Davy, C. Darcy, and N. Odling, 2002, A statistical model for fracture network geometry, with validation on a multiscale mapping of joint network (Hornelen Basin, Norway): Journal of Geophysical Research, v. 107

Brown, W., Grayson, R., 1985, Tectonism and Sedimentation in the Arbuckle Mountain region, Southern Oklahoma Aulacogen: Baylor Geological Society, AAPG Student Chapter, 43p.

Comer, J.B., 2005, Facies distribution and hydrocarbon production potential of Woodford Shale in the southern Midcontinent, in B.J. Cardott, ed., Unconventional energy resources in the southern Midcontinent, 2004 symposium: Oklahoma Geological Survey Circular 110, p. 51- 62.

Comer, J. B., 2008, Woodford Shale in southern midcontinent, USA—Transgressive system tract marine source rocks from arid passive continental margin with persistent oceanic upwelling: AAPG, Search and Discovery Article #90078

Cardott, B, J., 2012, Thermal maturity of Woodford Shale gas and oil plays, Oklahoma, USA: *International Journal of Coal Geology,* v. 103, p. 109-119

Cardott, B. J., 2007, Overview of Woodford gas-shale play in Oklahoma: Oklahoma Geological Survey, Woodford Gas Shale Conference

Cardott, B. J., Lambert, M.W., 1985, Thermal maturation by vitrinite reflectance of Woodford Shale, Anadarko Basin, Oklahoma; The American Association of Petroleum Geologists Bulletin, v. 69, No. 11

Clark, J., 2015: Imaging fractures in outcrops of Chattanooga Shale in the Wills Valley Anticline with terrestrial LiDAR (Master's Thesis): The University of Alabama

Cox, R. T., VanArsdale, B. R., 1988, Structure and Chronology of the Washita Valley fault, Southern Oklahoma Aulacogen: Shale Shaker, July, August, p.2- 13.

Decelles, P.G.; and Giles, K.A., 1996, Foreland basin systems: Basin Research, v. 8, p. 105-123.

Dershowitz, W. S., and H. H. Einstein, 1988, Characterizing rock joint geometry with joint system models: Rock Mechanics and Rock Engineering, v. 21, p. 21–51,

Dershowitz, W.S., Herda, H.H., 1992, Interpretation of fracture spacing and intensity, in Proceedings of the 33rd U.S. Symposium on Rock Mechanics, Tillers, J. R., Wawersik, W. R., Eds., pp. 757-774

Engelder, T., 1985, Loading paths to joint propagation during a tectonic cycle: an example from the Appalachian Plateau, U.S.A, *Journal of Structural Geology,* v. 7, p. 459-476

Flawn, P. T., Goldstein, A., Jr., King, P. b, Weaver, C. E., 1961, The Ouachita System: Bureau of Economic Geology: University of Texas Publication 6120, p. 401

Ghosh, S., 2017, Integrated studied on Woodford Shale natural fracture attribute, origin, and their relation to hydraulic fracturing (PhD Thesis): University of Oklahoma

Graham, S. A., Ingresoll, R. V., and Dickinson, W. R., 1976, Common provenance for lithic grains in Carboniferous sandstones from Ouachita Mountains and Black Warrior Basin: Journal of Sedimentary Research, v. 46, no. 3, p. 620-632

Guerriero, V., S. Vitale, S. Ciarcia, and S. Mazzoli, 2011, Improved statistical multiscale analysis of fractured reservoir analogues: Tectonophysics, v. 504, p. 14–24

Hackley, P., and Cardott, B., 2016, Applications of organic petrography in North American shale petroleum systems: A review; International Journal of Coal Geology, v. 163, p. 8-51

Hanzel, J., 2012, LiDAR Based fracture characterization: An outcrop scale study of the Woodford shale, McAlister shale pit, Oklahoma (Master's Thesis): Oklahoma State University

Hodgetts, D. 2012, Laser scanning and digital outcrop geology in the petroleum industry: A review. Marine and Petroleum Geology, 46, pp. 335-354

Houseknecht, D., et al., 2014, Upper Devonian-Mississippian stratigraphic framework of the Arkoma Basin and distribution of potential source-rock facies in the Woodford-Chattanooga and Fayetteville-Caney shale-gas systems: *AAPG Bulletin*, v. 98, p. 1739-1759

Houseknecht, D. W., and C. Spötl, 1993, Empirical observations regarding methane deadlines in deep basins and thrust belts, in D. G. Howell, ed., The Future of Energy Gases, U.S. Geological Survey, Professional Paper 1570, p. 217–231

Houseknecht, D., 1984, Evolution from passive margin to foreland basin: the Atoka Formation of the Arkoma Basin, south-central U.S.A.: *The International Association of Sedimentologists*

Jackson, C. P., A. R. Hoch, and S. Todman, 2000, Self-consistency of heterogeneous continuum porous medium representation of fractured medium: Water Resources Research, v. 36, p. 189–202

Ji, S., Saruwatari, K. 1998, A revised model for the relationship between joint spacing and layer thickness, Journal of Structural Geology, 20, 11, pp. 1495-1508

Johnson, D. M., Hooper, P. R., and Conrey, R. M., 1999, XRF Analysis of Rocks and Minerals for Major and Trace Elements on a Single Low Dilution Li-tetraborate Fused Bead; Advances in X-ray Analysis, v. 41, p. 843-867

Kirkland, D.W., R.E. Denison, D.M. Summers, and J.R. Gormly, 1992, Geology and organic geochemistry of the Woodford Shale in the Criner Hills and western Arbuckle Mountains, in K.S. Johnson and B.J. Cardott, eds., Source rocks in the southern Midcontinent, 1990 symposium: Oklahoma Geological Survey Circular 93, p. 38-69

Kon, Y., Murakami, H., Takagi, T., and Watanabe, Y., 2011, The development of whole rock analysis of major and trace elements in XRF glass beads by fsLA-ICPMA in GSJ geochemical reference samples: Geochemical Journal, v. 45, p. 387-416

Kont, M., 1991, Distribution and depositional system of spiro sandstone in Arkoma Basin of Eastern Oklahoma (M.S. Thesis): Oklahoma state university

Kvale, E. P.,. Bynum, J., 2014, Regional Upwelling During Late Devonian Woodford Deposition in Oklahoma and its Influence on Hydrocarbon Production and Well Completion: AAPG Education Directorate, Oklahoma City, Oklahoma, May 29, 2014

Ladeira, F.L., Price, N.J. 1981, Relationship between fracture spacing and bed thickness, Journal of Structural Geology, 3, 2, pp. 179-183

Long, J. C. S., J. S. Remer, C. R. Wilson, and P. A. Witherspoon, 1982, Porous media equivalents for networks of discontinuous fractures: Water Resources Research, v. 18, p. 645–658

Lowe, D. R., 1975, Regional controls on silica sedimentation in the Ouachita system: Geological Society of America Bulletin, v. 86, p. 1123–1127

Mauldon, M., W. M. Dunne, and M. B. Rohrbaugh Jr., 2001, Circular scanlines and circular windows: new tools for characterizing the geometry of fracture traces: Journal of Structural Geology, v. 23, p. 247–258

Mazzullo, S.J.; Wilhite, B.W.; and Boardman, D.R., II, 2011, Lithostratigraphic architecture of the Mississippian Reeds Spring Formation (middle Osagean) in southwest Missouri, northwest Arkansas, and northeast Oklahoma: outcrop analog of subsurface petroleum reservoirs: Shale Shaker, v. 61, p. 254-269

McCaffrey, K.J.W., Jones, R.R., Holdsworth, R.E., Wilson, R.W., Clegg, P., Imber, J., Holliman, N., and Trinks, I., 2005, Unlocking the spatial dimension: Digital technologies and the future of geoscience fieldwork: Journal of the Geological Society of London, v. 162, no. 6, p. 927–938

Miall, A.D., 1995, Collision-related foreland basins, in Busby, C.J.; and Ingersoll, R.V., eds., Tectonics of sedimentary basins: Blackwell Science, Cambridge, Massachusetts, p. 393-424.

Milad, B., Slatt, R., 2017, Integrated 3-D Seismic, outcrop, and core data for characterization of natural fractures of the Hunton limestone and the Woodford shale in central Oklahoma: in Proceedings, AAPG annual convention and exhibition, Houston, Texas, April 2-5 2017, v. 51382

Minisini, D., Wang, M., Bergmann, S.C., Aiken, C. 2014, Geological data extraction from LIDAR 3-D photorealistic models: A case study in organic-rich mudstone, Eagle Ford Formation, Texas. Geosphere, 10, 3: 610-626

Mnich, C., 2009, Geochemical signatures of stratigraphic sequences and sea-level change in the Woodford shale, Permian Basin (PhD Dissertation): University of Oklahoma

Narr, W., 1996, Estimating Average Fracture Spacing in Subsurface Rock, AAPG Bulletin, 80, 10, pp. 1565-1586

Narr, W., Lerche, I., 1984, A Method for Estimating Subsurface Fracture Density in Core, AAPG Bulletin, 68, 5, pp. 637-648

Nelson, R., 1985, Geologic analysis of naturally fractured reservoirs: Petroleum Geology and Engineering, Gulf Publishing Co., 320p

Norrish, K., and Hutton, J. T., 1969, An accurate X-ray spectrographic method for the analysis of a wide range of geological samples: Geochem, Cosmochem, Acta, v. 33, p. 431-453

Olariu, M.I., Ferguson, J.F., Aiken, C.L.V., Xu, X., 2008, Outcrop fracture characterization using terrestrial laser scanners: Deep-water Jackfork sandstone at Big Rock Quarry, Arkansas, Geosphere, 4, 1, pp. 247-259

Parrish, J. T., 1982, Upwelling and petroleum source beds, with reference to Paleozoic: AAPG Bulletin, v. 66, p. 750–774.

Pearce, M.A., Jones, R.R., Smith, S.A.F., McCaffrey, J.W., 2011, Quantification of fold curvature and fracturing using terrestrial laser scanning, AAPG Bulletin, 95, 5, pp. 771-794

Perry, J., 1995, Arkoma Basin Province: National assessment of United States oil and gas resources – Results, methodology, and support, i. 62, p. 1-17

Portas, R. M., 2009, Characterization and Origin of Fracture patterns in a Woodford Shale quarry in southeastern Oklahoma for Application to Exploration and Development (Master's Thesis): University of Oklahoma

Portas, R. M., Slatt, R., 2010, Characterization and Origin of Fracture patterns in a Woodford Shale quarry in southeastern Oklahoma for Application to Exploration and Development; In Proceedings, AAPG Annual Convention, New Orleans, Louisiana, April, 2010

Priest, S. D., 1993, Discontinuity analysis for rock engineering: London, United Kingdom, Chapman & Hall, 473 p

RIEGL, 2021, http://www.rieglusa.com/index.html,

Schiopfer, M.P.J., Arslan, A., Walsh, J.J., Childs, C., 2011, Reconciliation of contrasting theories for fracture spacing in layered rocks, Journal of Structural Geology, 33, pp. 551-565

Slatt, R., Portas, R., Buckner, N., Abousleiman, Y., O'Brien, N., Tran, M., Sierra, R., Philip, P., Miceli-Romero, A., Davis, R., and Wawrzyniec, T., 2011, Outcrop/behind outcrop (quarry), multiscale characterization of Woodford gas shale: In Proceedings, AAPG International Conference, Calgary, Alberta, September 12-15, 2010

Slatt, R., McCullough, B., Molinares, C., Baruch, E., Turner, B., 2015, Paleotopographic and Depositional environment controls on "sweet spot" locations in unconventional resource shales: Woodford and Barnett shale examples: Part 2: in Proceedings, AAPG Annual Convention and Exhibition, May-June 2015, v. 80467,

Spotl, C., Housknecht, D.W., Jaques, R., 1998, Kerogen maturation and incipient graphitization of hydrocarbon source rocks in the Arkoma Basin, Oklahoma and Arkansas: a combined petrographic and Raman spectrometric study: *Organic Geochemistry*, v. 28, i. 9-10, p. 535-542

Stearns, D. W., 1968, Certain aspects of fractures in naturally deformed rock, *in* Riecker (ed), NSF advanced Science Seminar in Rock Mechanics, Air Force Cambridge Research Laboratories

Suarez-Ruiz, I., Flores, D., Graciano Mendonca Filho, J., and Hackley, P., 2012, Review and update of the applications of organic petrology: Part 1, geological applications; Journal of Coal Geology, v. 99, p. 54-112

Suneson, N., 2012, Arkoma Basin Petroleum – Past, Present, and Future, a Geologic Journey Through the Wichita's, Black Mesa Basalt, and much more: *Shale Shaker*, v. 63, p.38-70

Sutherland, P., 1988, Late Mississippian and Pennsylvanian depositional history in the Arkoma basin area, Oklahoma and Arkansas: *Geological Society of America Bulletin,* v. 100, p. 1787-1802

Thomas, W. A., 2004, Genetic relationship of rift-stage crustal structure, terrane accretion, and foreland tectonics along the southern Appalachian-Ouachita orogen: Journal of Geodynamics, v. 37, p. 549-563

Twiss, R. J., Moores, M. E., 1992, Structural Geology: W. H. Freeman and Company Publishing, 532 p.

Tóth, T. M., 2010, Determination of geometric parameters of fracture networks using 1-D data: Journal of Structural Geology, v. 32, p. 1271–1278.

Viele, G. W., and Thomas, W. A., 1989, Tectonic synthesis of the Ouachita orogenic belt, The Appalachian-Ouachita orogen in the United states: Geological Society of America, The Geology of North America, v. F-2, p. 695-728

Walper, J.L., 1977. Paleozoic tectonics of the southern margin of North America Gulf Coast Assoc. Geol. Soc. Trans. 27, 230–241.

Wickham, J., Roeder, D., Briggs, G., 1976, Plate tectonics models for the Ouachita fold belt: Geology, v. 4 (3), p. 173-176

Wilson, C.E., Aydin, A., Karimi-Fard, M., Durlofsky, L.J., Sagy, A., Brodsky, E.E., Kreylos, O., Kellog, L.H., 2011, From outcrop to flow simulation: Constructing discrete fracture models from a LIDAR survey, AAPG Bulletin, 95, 11, pp. 1883-1905

Wu, H., Pollard, D.D. 1995, An experimental study of the relationship between joint spacing and layer thickness, Journal of Structural Geology, 17, 6, pp. 887-905.

Xu, C., Cronin, T., McGinness, T., Steer, B., 2009, Middle Atokan sediment gravity flows in the Red Oak field, Arkoma Basin, Oklahoma: A sedimentary analysis using electrical borehole images and wireline logs: *AAPG Bulletin,* v. 93, no. 1, p. 1-29

Xu, X., Aiken, C., Bhattacharya, J.P., Corbeanu, R.M., Nielsen, K.C., McMechan, G.A., and Abdelsalam, M.G., 2000, Creating virtual 3-D outcrops: The Leading Edge, v. 19, p. 197–202

Younes, A. I., and Engelder, T., 1999, Fringe cracks: key structures for the interpretation of the progressive Alleghanian deformation of the Appalachian plateau: Geological Society of America Bulletin, v. 111, no. 2, pp. 219-239

Zahm, C.K., Zahm, L.C., Bellian, J.A., 2010, Integrated fracture prediction using sequence stratigraphy within a carbonate fault damage zone, Texas, USA, Journal of Structural Geology, 32, pp. 1363-1374.

Zeeb, C., E. Gomez-Rivas, P.D. Bons, and P. Blum, 2013. Evaluation of sampling methods for fracture network characterization using outcrops: AAPG Bulletin, 97(9), p. 1545–1566, doi: 10.1306/02131312042.

APPENDIX A

LiDAR WORKFLOW

1. Initial machine setup

- Attach LiDAR to tripod, mount camera on LiDAR, connect all cables

2. Open RiSCAN Pro and create a new project

3. Set up camera

- Camera configuration (V-line) -> Automatic to acquire settings -> set back to Manual

4. Set Reflector Type

- Right click ‘Calibrations’ select ‘New Reflector’
- Reflector color = Silver Diameter = .05m Reflector Shape = Sphere

5. Establish New Single Scan

- Right click Scan position select ‘New Single Scan’
- For initial scan click ‘Panorama’. Set resolution to desired settings. (I usually do .05 but can be played around with)

6. Identify and Mark Tiepoints.

- This can be done automatically but I prefer to do it manually
- Right click ‘Tiepoints’ and select ‘New Tiepoints’ then mark all tiepoints
- It helps if the newly acquired image is opened with ‘Linear Scaled’

7. Fine-scan Tiepoints

- Open up TPL (SOCS) and select all the tiepoints then choose ‘finescan selected tiepoints’

8. Register and Find Corresponding Tiepoints

- Copy newly fine-scanned tiepoints to TPL (PRCS) then highlight and select ‘Tiepoints are control points’
- Then from TPL (PRCS) copy the tiepoints over to TPL (GLCS)
- Once this is done head back to TPL (SOCS) and highlight the tiepoints then select ‘Find Corresponding Points’

9. Additional High-resolution scans of Specific Areas for High Quality Images

- Right click on the initial scan and select ‘New Single Scan’
- Select area of interest by holding the ‘Alt’ key and highlighting desired area
- Increase resolution as high as possible for better results (In lab test .002 seemed good although .001 seemed to push the limits of the machine too far)

APPENDIX B

LIDAR SYSTEMS

Parameter	3D Terrestrial Laser Scanner Series				
	VZ-6000	VZ-4000	VZ-2000	VZ-1000	VZ-400
Key Elements	Ultra long range, high speed	Very long range, high speed	Long range, very high speed	Long range, accurate, extra high speed	High accuracy, extra high speed
Max Range @ 80% Reflectivity	5800 m	3900 m	1950 m	1350 m	550 m
Minimum Range	5 m	5 m	2.5 m	2.5 m	1.5 m
Accuracy	15 mm	15 mm	8 mm	8 mm	5 mm
Measurement Rate	up to 222K measurements per second	up to 222K measurements per second	up to 400K measurements per second	up to 122K measurements per second	up to 122K measurements per second
Vertical Angular Stepwidth	0.002°	0.002°	0.0015°	0.0024°	0.0024°
Horizontal Angular Stepwidth	0.002°	0.002°	0.0024°	0.0024°	0.0024°

Differences in LiDAR laser scanners, VZ-400 model used in this study highlighted (Clark, 2015).